USING KITES FOR METEOROLOGICAL MEASUREMENT OF THE TROPICAL MARINE BOUNDARY LAYER

A THESIS SUBMITTED TO THE GRADUATE DIVISION OF THE
UNIVERSITY OF HAWAIʻI AT MĀNOA IN PARTIAL FULFILLMENT
OF THE REQUIREMENTS FOR THE DEGREE OF

MASTER OF SCIENCE

IN

ATMOSPHERIC SCIENCES

AUGUST 2018

By

David John DeCou

THESIS COMMITTEE:

Alison D. Nugent, Chairperson
Jennifer Griswold
Yi-Leng Chen

ACKNOWLEDGMENTS

I would like to express my deepest thanks to my advisor and committee chair, Dr. Alison D. Nugent, who has continuously given me guidance, advice, and encouragement. Through her ever-present support over the course of my graduate education, she has inspired and helped me directly to improve my presentation skills, writing/organizational skills, coding skills, and research skills. Without her experience, expertise, materials, and ideas, this project would not have been possible. I owe my success in this program to her support.

I would also like to thank both Dr. Jennifer Griswold and Dr. Yi-Leng Chen for their helpful critique of my thesis and participation in my defense. Their input has greatly improved my work and led to deeper discussion in this project. My scientific writing and overall organization has improved as a result of their help. In addition, Dr. Griswold's Satellite Applications class has provided me with valuable coding experience in Matlab that helped me in the data analysis for this project significantly. Her class has helped me become more familiar with coding in general.

I would also like to sincerely thank the Department of Atmospheric Sciences at the University of Hawai‘i at Mānoa for providing me with financial support as a graduate teaching assistant during my education here. My time at UH has provided me with valuable experience teaching, which has helped me build my communication and public speaking skills.

Special thanks to Emily Tashiro for her great help and support during the editing and revising process.

ABSTRACT

Kite-based platforms to measure atmospheric properties have been used for centuries. With rapid development of new miniaturized sensor technology, kites may once again be utilized in atmospheric research. In this study, kites are found to be advantageous due to their low cost and capability for long-duration, continuous flights, which enable long-duration in-situ observation. We use our strategic location on the island of O‘ahu in Hawai‘i to make meteorological measurements of the steady incoming trade wind flow from the windward coast. Incoming marine air is measured from the coastline with instruments tethered to a kite string, giving information on trade wind flow properties, such as air temperature and humidity, for use in studying the marine boundary layer. We observe high-resolution vertical profiles and horizontal temporal variations of the atmospheric temperature and humidity. Temporal and vertical variation can also be observed by flying multiple instruments simultaneously at different heights within the marine boundary layer. Using a kite platform, we observe small-scale, strongly anticorrelated temperature and humidity perturbations at constant altitudes greater than 300 m above sea level. These anticorrelated variations are hypothesized to be important for convective initiation, following Nugent and Smith (2014).

TABLE OF CONTENTS

LIST OF TABLES

LIST OF FIGURES

CHAPTER 1: INTRODUCTION

1.1 Background

The Hawaiian Islands (160˚W 21˚N) in the Central Pacific are immersed in steady easterly or northeasterly trade wind flow throughout much of the year. As these trade winds cross the islands, they are modified in a number of ways by the land surface. In the lowest layer of the atmospheric boundary layer, frictional drag slows and deflects the trade winds as the air interacts with the terrain and other obstacles on the rough island surface. In addition, the land surface warms more rapidly than the ocean surface during the day and cools more rapidly during the night due to the land's smaller heat capacity as compared to water. This creates horizontal temperature differences, which generate local diurnal wind circulations called sea- and land-breezes that may interact with the trade winds at low levels. A goal of this study is to take measurements characteristic of the upstream trade wind flow before it is modified by the island environment of Oʻahu, and use these measurements to study the marine boundary layer, which lies within the lowest 2 km of the atmosphere (Winning, Chen, & Xie, 2016). The atmospheric conditions within this layer are important to study because they play a role in the development of clouds, convection and rainfall over the Hawaiian Islands (Gaimbelluca and Nullet, 1991). For example, if the boundary layer air is moist and unstable, this can contribute to the convective development of the air lifted over the mountains and can ultimately be responsible for generating mountain showers.

In this study, we seek to observe small variations in temperature and humidity within the upstream low-level trade winds that may determine the temporal and spatial distribution of convection over the region. There are many platforms that can be used to sample the atmospheric

boundary layer, including aircraft, balloons, kites and drones. We have found that kites offer several practical advantages to our study in particular, due to the prevalence of steady trade wind conditions throughout the year. Steady winds allow kites to be reliably deployed whereas balloons and drones are best in light winds. Cost is an additional factor, which eliminates our ability to use aircraft. Based primarily on these two factors, this study will focus on the use of kites for observing the marine boundary layer. Historical kite use, both early (Section 1.1.1) and recent (1.1.2) will be described in the following sections, followed by the study objectives in Section 1.2.

1.1.1 Historical Background

Kite-based platforms were among the first platforms used in attempts to study the atmosphere, and have been utilized for over 200 years. In 1749, Dr. Alexander Wilson from the University of Glasgow made the first observations of the lower atmosphere by attaching thermometers to a series of paper kites (Wiche, 1992). There were 6 kites total, ranging from 4 to 7 feet in length, attached at intervals in tandem to a single string. Thermometers were attached via burning wicks of different lengths so they would drop at varying altitudes above the Earth's surface. These thermometers were wrapped in wads of paper so they would not break as they struck the ground. After falling, they would be quickly collected and have their temperature read to obtain a rough sounding of the first few hundred feet of the troposphere. Other atmospheric studies using similar paper kites followed over the next century. In 1822, a kite was used to study temperature lapse rates in the Arctic by lifting self-registering thermometers that marked the minimum recorded temperature (Gold and Harwood, 1909). In 1840, kites were used to study cloud base heights and properties (Espy, 1841). In 1884, a series of kites flown in tandem raised

a self-recording anemometer to profile the winds over 1300 feet (Archibald, 1884). In 1885, the Blue Hill Observatory at Harvard became a major site for kite research, initially to study the atmospheric electrical field (McAdie, 1892, 1917; Gold and Harwood, 1909). In 1894, kites were used at Blue Hill Observatory to fly the first recording thermograph (Fergusson, 1933). This was followed a year later by the successful launch of a meteorograph, another type of self-recording instrument. The meteorograph weighed roughly 2 lbs, containing a chart wrapped around a rotating cylinder that automatically recorded pressure, temperature, humidity, and wind velocity (Wiche, 1992).

In 1895, the United States Weather Bureau (now the National Weather Service) officially began using kites to study the atmosphere (Wiche, 1992). Initially, modified Malay kites were utilized, but were quickly discarded in favor of the more stable Hargrave box kites (Figure 1).

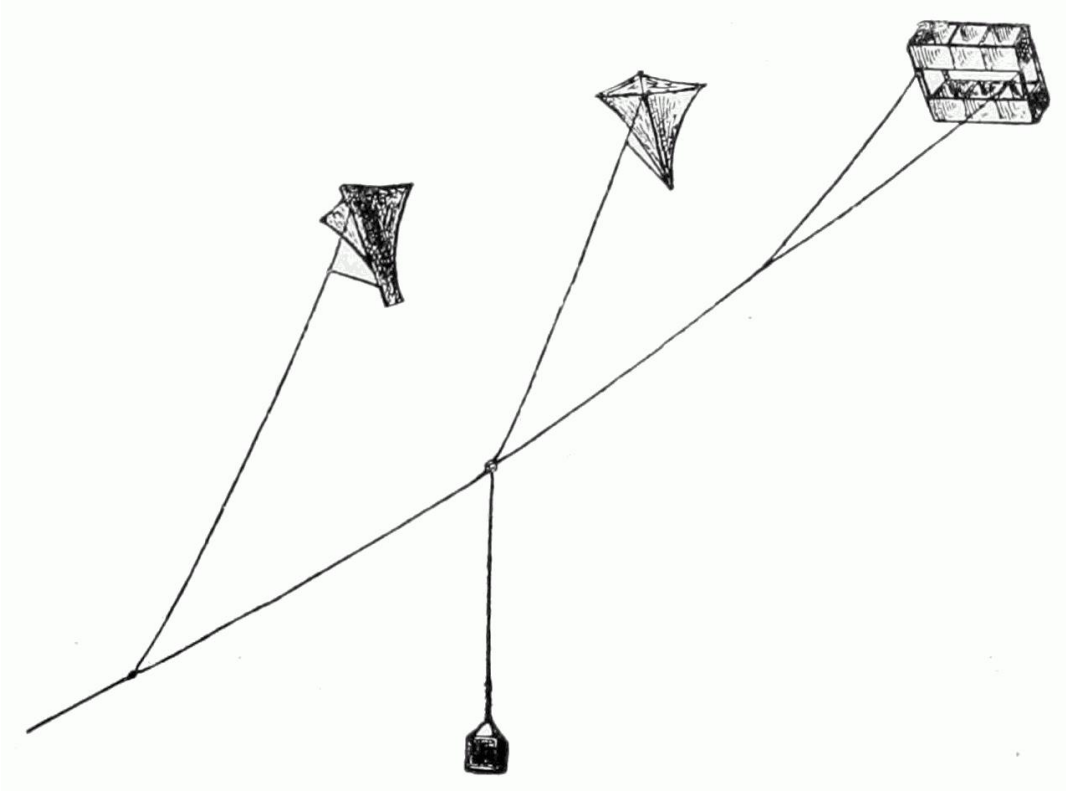

Figure 1. Reproduced from Varney (1898). An illustration of three different types of early meteorological kites flown in tandem, carrying a meteorograph. The kite on the left is a Malay kite, the central kite is a modified Malay kite, and the kite on the right is a Hargrave box kite.

In 1898, the Weather Bureau began taking daily simultaneous observations of the lower atmosphere at 17 official kite stations across the Central and Eastern United States (Frankenfield, 1900). The altitudes of kite-borne meteorographs were estimated by taking into account the length of the deployed kite line, the angular elevation of the lead kite, and the angle of the wire at the reel, which could be used to estimate the amount of curvature in the line. Measurements were made at roughly 500-foot intervals, although occasionally winds were too light to fly kites (Wiche, 1992). Additional kite stations for the U.S. Weather Bureau were established in 1917 due to an increasing need for upper-air data with the onset of World War I. However, by May of

1933, the U.S. Weather Bureau had ceased all official kite operations due to an increasing amount of air traffic, a lack of sufficient altitude measurements and reliability, and an improvement in weather balloon sounding technology (Balsley et al., 1998).

1.1.2 Recent Kite Studies

In recent decades, kites have been used for numerous boundary layer studies and vertical profiling experiments, as more modern platforms are being developed. In 1980-81, a kite study of the boundary layer winds at Kahuku Beach on Oʻahu was done with four sets of two automatically-recording TALA (tethered aerodynamically lifting anemometer) kites flying continuously at 100 and 300 feet, used concurrently with several handheld kites for data comparison (Daniels and Oshiro, 1982). Long-term wind speeds were estimated at the Kahuku coastal plain for the purposes of surveying the location for potential wind power development. Turbulence and boundary layer properties were also studied and characterized. Kahuku Wind Farm has been operating in the location since early 2011 (Hawaii State Energy Office, 2018).

In 1990, another field campaign used specially designed kites carrying electrometers to fly up to 3.5 km height on Christmas Island. This was part of a University of Colorado Cooperative Institute for Research in Environmental Studies (CIRES) program to measure the global atmospheric electric field during fair-weather conditions (Balsley et al., 1992). The platform consisted of up to 4 separate parafoil kites that could be attached in tandem to a 6-km length of 900-lb test Kevlar tether line. Parafoil kites have a series of open-ended air-filled pockets to hold them aloft, and generally contain no rigid parts. In this study, each parafoil had an area of 12.5 m^2 and was used to lift a series of spherical 30.5-cm-diameter containers that held modified

rawinsondes and electrometers to provide pressure, temperature, humidity, and electrical field information.

The CIRES group carried out further kite research in other locations around the world, and developed a device called a wind tram that is capable of carrying an instrument payload up and down the kite string (Balsley et al., 1998). The kite is used as an anchor in the sky, remaining stable in a relatively fixed position while the radio-controlled wind tram moves up and down the line, powered by the wind. Using this platform, vertical profiles of atmospheric variables can be observed. CIRES later used a similar system to study extreme gradients in the nocturnal boundary layer in southeastern Kansas, using kites to carry a series of lightweight instruments for collection of continuous in-situ data (Balsley et al., 2003). 1-Hz profiles of temperature, pressure, humidity, and wind data were collected up to 450 m. Balloons were also used in this study in low wind conditions, while kites were used in moderate to high wind conditions.

Kites were similarly used in conjunction with balloons in the study of an ozone-rich plume as part of the North Atlantic Regional Experiment (NARE) at Ferryland Downs, Newfoundland, Canada (Knapp et al., 1998). In this study, 65 vertical profiles of ozone mixing ratio, water vapor mixing ratio, and temperature were obtained using a combination of tethered balloons and kites as observation platforms. Parafoil kites with areas of 5 m^2 and 15 m^2 were used in addition to a 10 m^2 Sutton Flowform kite. Kites were used in place of tethered balloons when wind conditions were too strong. This was also the case in Bain et al. (2010), where West African monsoon-associated nocturnal boundary layer structure was observed. Here, tethered balloons and kites profiled the boundary layer over central Sahel up to 200 m, using a parafoil kite in high winds (>10 m s^{-1}) when balloons could not be flown. Measurements of pressure, temperature, and

relative humidity were obtained using a tethersonde package at 1.5 Hz resolution. The instrument package also had a mounted anemometer to provide measurements of wind speed and direction.

Kites were also used in an Antarctic boundary layer study of fine-scale atmospheric structure, where high-resolution profiles of winds and potential temperature were compared to Sodar-measured acoustic backscatter profiles (Anderson, 2002). The wind and potential temperature profiles are collected using a modified kite-borne tethersonde. The sonde itself was originally designed for use with a blimp, but it was found to be unsuitable for work in Antarctic temperatures (< -10°C). In Anderson (2002), the instrument was attached 10 m below the kite, and took wind speed measurements using a three cup anemometer, while temperature was taken by a shielded bead thermistor. A Rokkaku kite, which is a traditional six-sided Japanese kite, was used for wind speeds over 3 m s^{-1}, while a kite-balloon hybrid was used for nearly calm conditions.

Finally, a parafoil kite-based observation system was used to measure concentrations of particulate matter over the grasslands of Inner Mongolia (Reiche et al., 2011). In this study, a 4 m^2 kite was used, capable of lofting roughly 6 kg of equipment in wind speeds between 3 and 20 m s^{-1}. A self-adjusting platform was designed and also utilized for carrying a portable Environmental Dust Monitor, an anemometer, and a GPS receiver. This platform was used to take profiles of particular matter fluxes below 100 m altitude.

The studies described here are examples where kite platforms were used, but it is not an exhaustive list. The kite-based studies described have several things in common. First, most of these studies take place in locations that are either remote (Christmas Island, Central Sahel, Inner Mongolia, Antarctica), or where winds are relatively steady (Christmas Island, Oʻahu). In addition, several of these studies use kites to support a tethered balloon system in higher wind

environments. Other studies use a series of kites flown in tandem to obtain additional lift. This is needed, in addition to a strong tether, when the instrumentation includes heavy payloads.

1.2 Study Objectives

Recent advances in technology provide new possibilities for kite-based measurements. Meteorological sensors can now be made smaller, lighter, and cheaper than before, and are thus suitable for kite platforms. The current study uses small, newly-developed UAV (unmanned aerial vehicle) sensors attached at fixed lengths along a single kite string to measure atmospheric properties at multiple altitudes simultaneously. These sensors directly measure temperature, relative humidity, pressure, and GPS position (latitude, longitude, and altitude) with 1 Hz frequency or 1 second temporal resolution. The kite-borne sensors are flown off of O‘ahu’s windward coast, measuring properties of the incoming trade winds as they come upon the coastline (Figure 2). Other observation platforms have been considered for use in this study, but kites are more cost-effective, more easily deployed, and more easily retrieved than other options. For example, small UAV rotorcraft drones are popular in recreational use and are capable of carrying small meteorological sensors. However, they are more costly than kites, are limited by a short battery life (typically < ~30 mins), and have an even shorter battery life or flight errors when winds are high. Kite observing is only limited by the battery life of the attached sensors. Tethered balloons are viable in that they allow for multiple simultaneous measurements along the tether and can attain high altitudes, but they are more costly and cumbersome than kites. In addition, they have proven difficult to fly in high wind environments (Balsley at el., 2003, Bain et al., 2010, Knapp et al., 1998) due to the wind drag on the balloon itself.

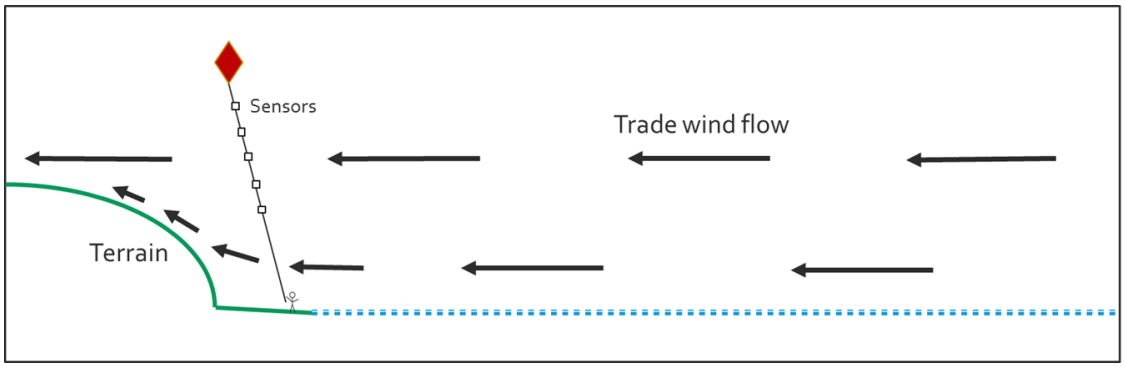

Figure 2. An illustration of this study's kite sampling method in relation to the ambient trade wind flow moving on-shore. The blue dashed line represents the ocean surface, and the green solid line represents the island terrain. The vectors represent the trade wind direction and magnitude relative to the coast. The red diamond and contiguous solid black line represent the kite and kite string, with the boxes along the string representing the sensors attached to it.

The main goals of our study are:

1) Develop the skills and tools necessary for using kites to take high quality marine boundary layer observations. This includes the development of platform components, as well as methods of kite deployment, retrieval and sensor attachment.
2) Use the kite platform to take measurements of the incoming trade winds within the mixed boundary layer and observe variations in ambient air temperature and humidity at a constant altitude.
3) Search for evidence of moist "seeds" of convection within the incoming flow and apply our observations to the study of island convective initiation.

1.2.1 Convective Initiation Background

In a 2014 paper by Nugent and Smith (hereafter NS14), anticorrelated fluctuations in air temperature (T) and specific humidity (q_v) are observed in the undisturbed trade wind flow upstream of the tropical island of Dominica, at 300 m altitude. These anticorrelated patches are theorized to be important for convective initiation, following Woodcock's theory of moist convective initiation (Woodcock, 1960). Woodcock proposed that humidity variations in the ambient flow may play a role in orographic convection. As an inhomogeneous layer of air is lifted, moist parcels in the layer will be the first to reach their respective lifting condensation levels (LCL) and become saturated. The moist parcels will then develop buoyancy with respect to the surrounding drier air due to the release of latent heat (Figure 3). In NS14, this idea is applied to observations from the Dominica Experiment (DOMEX) field campaign. Models are

used to uniformly lift a layer containing observed anticorrelated T and q_v patches and calculations are performed of the resulting differential buoyancy and accelerations (NS14).

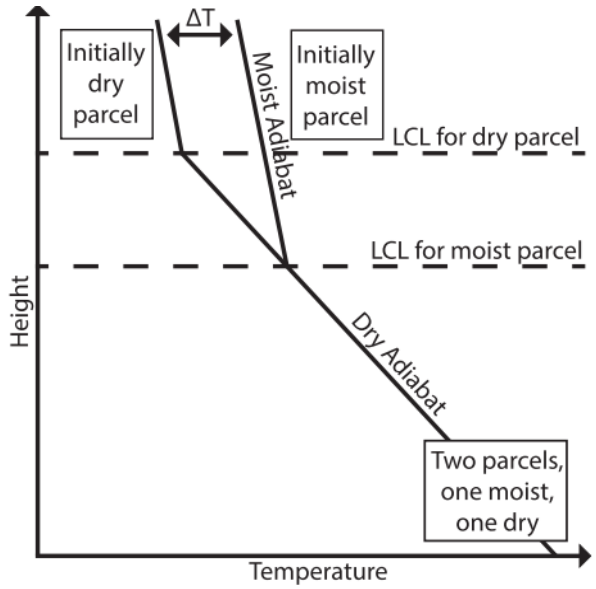

Figure 3. From Nugent and Smith, 2014. A simple schematic illustrating the resulting temperature and buoyancy differences after two parcels of differing moisture amounts are lifted the same distance. The moist parcel reaches its LCL first, becoming warmer, and therefore more buoyant with respect to the drier parcels.

In NS14, the anticorrelated variations in T and q_v were found in the observational DOMEX aircraft datasets during an upstream flight track at a constant 300 m above sea level (Figure 4). The average correlation coefficient between T and q_v was -0.78 from all research flights in the absence of precipitation (NS14). In this upstream sub-cloud layer, the air was observed to typically be either warm and dry or cool and moist. These types of perturbations can be created

by several processes related to upstream trade wind convection. Warm, dry air can be entrained into the mixed boundary layer from turbulent mixing while cool, moist air is created by evaporation within rain shafts (NS14). Additionally, cloud-adjacent downdrafts may create regions of dry air, warmed by adiabatic expansion, while detrainment of air from the clouds themselves can create regions of cool, moist air (NS14). These dry and moist patches are theorized to drift passively in the flow and align themselves according to their density in a process called buoyancy sorting. The moist patches are of particular interest, as they may act as convection "seeds" when the layer is lifted by the higher island terrain. Because of their application to island convective initiation, we seek to observe moist convection "seeds" in the T and q_v variations in the undisturbed flow upstream of O'ahu, an island that has similar characteristics to Dominica.

Dominica is a small tropical Caribbean island (750 km^2) located in the Lesser Antilles archipelago (15°N, 61°W) with mountains that extend up to 1400 m. Most of the rainfall in Dominica is orographically forced, as the trade winds flow over the higher terrain of the island. O'ahu is a larger tropical island (1545 km^2) with shorter mountains (extending up to 1220 m) located in the Hawaiian Islands of the Central North Pacific Ocean (21.5°N, 158°W), and it also experiences orographic trade wind convection throughout the year.

Due to its size, comparable orography, and location in the trade wind belt, O'ahu is a suitable analog to Dominica for studying moist convective initiation. In the current kite study, we seek to measure the upstream temperature and moisture fields by using kites to lift instruments to altitudes of 300 m or greater. The altitude of 300 m is chosen as the minimum appropriate altitude to mirror the observational altitude from NS14, but higher altitudes are preferred in order to minimize frictional effects by the island. Instruments are kept at a relatively constant altitude

in order to observe variations in T and q_v in the incoming flow for the purposes of observing moist "seeds" of convection.

The observation and mapping of moist convective "seed" characteristics is important for several reasons. First, the detailed physical processes involved in convective initiation are not fully understood, yet convective initiation may be key to important precipitation processes. For example, it is not well known how warm rain can initiate so close to mountainous coastlines. Typically, the assumed timescales for precipitation formation are larger than those allowed by advection of the mean flow (Lau and Wu, 2003). A better understanding of the upstream environment that leads to island orographic convection and precipitation may improve our ability to forecast or predict precipitation in current and future climates. Improving our understanding of these sub-grid scale variations in temperature and specific humidity may also allow us to improve convective model parameterizations. Furthermore, anticorrelated regions of temperature and specific humidity were only recently discovered during DOMEX (NS14) in the Caribbean trade wind belt. Can we observe this same phenomenon elsewhere? If not, why not? In addition, moist convective "seeds" had only been observed via research aircraft-borne instruments, roughly 20 km upstream of the island coastline. Can we observe this phenomenon from the coastline itself? Can we observe it in the incoming flow from a stationary observation point? If this phenomenon can be observed again, how does it change with altitude, time, location, and environmental conditions? These questions and more will be addressed in the following chapters.

The following Chapter 2 covers the methods and datasets used for this study. Results will be presented afterwards in Chapter 3. Lastly, Chapter 4 will include conclusions and discussion.

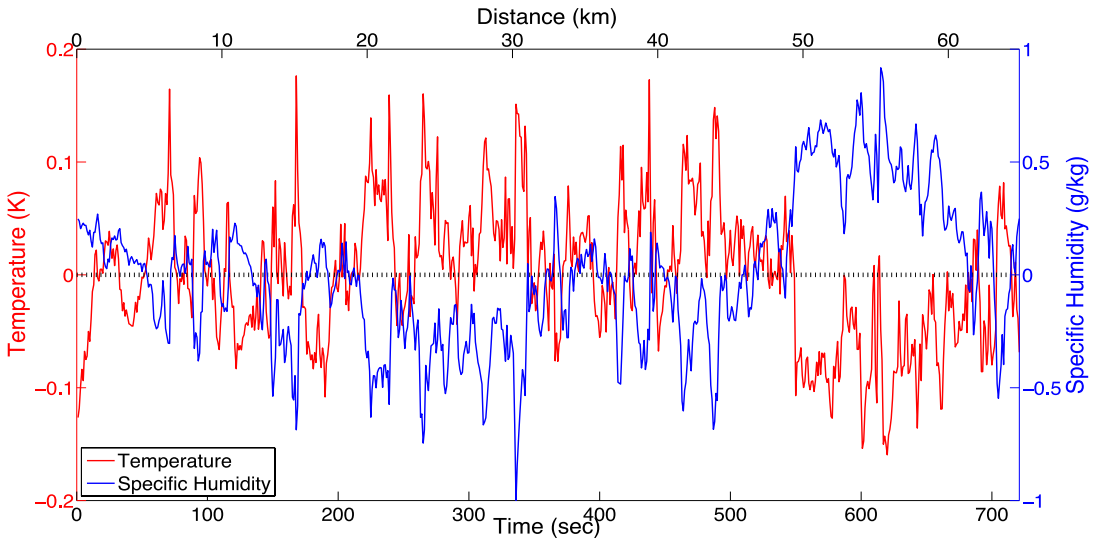

Figure 4. From Nugent and Smith 2014. Temperature (red) and specific humidity (blue) perturbations measured by aircraft along a flight leg upstream of Dominica at 300 m altitude during DOMEX. The correlation coefficient between the two curves for this case is -0.81.

CHAPTER 2: METHODS AND DATA

2.1 Kite Components

In developing a platform for use in boundary layer observation, a kite was needed that could achieve reasonable stability at high altitudes (> 300 m) for long duration (>1 hr) flights. Early tests used regular delta kites, but they were prone to diving, causing large changes in altitude and the potential to crash into the ground. Box kites were also used in early tests, but were difficult to launch. Due to this consideration, and successful tests with delta conyne kites, all subsequent tests used delta conyne platforms. Therefore, in all experiments described within this document, a single-line delta conyne kite was utilized (Figure 5). A delta conyne is a hybrid of a triangular delta kite and a box kite. The central 'box' portion of the kite contains a series of parallel struts that lend the kite added stability, while wings provide the kite additional lift. The size of the delta conyne kite used depends on the ambient wind speed environment; larger surface area kites are needed for additional lift on weak wind days. These are days where the mean ambient horizontal wind speed (U) is less than 3 m/s. On windier days (U > 5 m/s), smaller surface area kites are needed, as larger kites can generate too much lift, which places high tension on the line.

Figure 5. A photograph of a delta conyne kite used in early experiments for this study.

Our experiments require a thin line with low surface area to minimize drag, while also being strong enough to withstand kite tension in strong wind environments. We use Spiderwire Stealth® 65-lb test braided fishing line, because it achieves this balance of lightness and strength (Figure 6). Note that "65-lb test" refers to the tensile breaking strength of the line. In future flights, 80-lb test line will be used for additional durability. The line is composed of multiple thin Dyneema® fiber strings woven together for additional strength.

Figure 6. A photo of Spiderwire Stealth® 80-lb test braided fishing line that is attached to the kite. It is a slightly stronger line from the 65-lb test line used so far. A close-up of the line is provided for detail.

We wind this line onto a Tanacom 1000 electric fishing reel, which allows us to directly measure and control how much string is deployed, while also allowing us to reel the string in

smoothly with ease (Figure 7). This electric fishing reel is powered by a deep cycle 12V battery with a capacity of 79 ampere hours.

Figure 7. A photograph of the Tanacom 1000 electric fishing reel. The screen displays the deployed string length in meters. In the above example, 600.0 m of string is deployed.

2.2 Instrumentation

The instruments used with the kite platform in this study include Intermet's iMet-XQ UAV sensor as well as an upgraded prototype, the iMet-XQ2 (Figure 8), which recently became available. Intermet is a global supplier of radiosondes and other atmospheric sensors, including the XQ line of instruments. The XQ and XQ2 were originally designed to be used with rotary wing UAVs, but are suitable for use in kite-based observation due to their small size and weight. The XQ is 100 x 30 mm in area with a mass of 15 g. The XQ2 is 126 x 58 mm in area with a mass of 60 g. Both sensors directly measure temperature (°C) using a bead thermistor, relative humidity (%) using a capacitive sensor, and pressure (hPa) using a piezoresistive-type sensor. Each sensor type is also equipped with a GPS that provides information on time, date, and position (latitude, longitude, and altitude).

The XQ2 became available in January 2018 but had backorders well through March 2018 due to its popularity. It has several upgrades compared to the first version. It has an improved humidity sensor and a more accurate GPS, as well as a longer battery life (300 minutes) compared to the first (120 minutes). It is notably larger and heavier compared to the first, but is still capable of being easily fitted to the kite string and lifted by the kite. Further information on the response time, accuracy, and resolution of each sensor is provided in Table 1. Both sensors have a sampling resolution of 1 Hz and can store up to 16 Mb of data, which equates to 15 hours of observation. Data can be transferred to an external source via USB.

a.)

b.)

Figure 8. a.) A photograph of an iMet-XQ UAV Sensor, and b.) a photograph of an iMet-XQ2 UAV Sensor. The numbers written on the casings indicate the order in which the instruments were acquired.

Table 1. Summary of iMet-XQ and iMet-XQ2 humidity, temperature, pressure, and GPS sensor specifications. This includes the response time, accuracy, and resolution of each sensor type. Certain specifications are dependent on the ambient wind speed, which is included in the table.

Sensor	**Humidity**	**Temperature**	**Pressure**	**GPS**
XQ Resp. Time	5 s (1 m/s flow)	2 s	10 ms	1 s
XQ Accuracy	+/- 5% RH	+/- 0.3°C	+/- 1.5 hPa	N/A
XQ Resolution	0.7% RH	0.01°C	0.02 hPa	N/A
XQ2 Resp. Time	0.6 s	1 s (5 m/s flow)	10 ms	1 s
XQ2 Accuracy	+/- 5% RH	+/- 0.3°C	+/- 1.5 hPa	12 m vertically
XQ2 Resolution	0.1% RH	0.01°C	0.01 hPa	N/A

2.3 Instrument Attachment

While the iMet-XQs are sufficiently light to be carried upward by the kite, it was not immediately obvious how or where to attach them on the kite platform. The iMet-XQ in early tests was fixed to the kite itself but adding additional weight unevenly to the kite appeared to sometimes destabilize it during flight. Later tests have the sensors attached to the string itself rather than to the kite. As additional sensors were acquired for the project, it was found that attaching them at fixed lengths along the string could pose kite-unique observational benefits. With multiple simultaneous observations along the kite string, we may obtain high vertical resolution atmospheric profiles. However, we could not directly tie the kite string to the instruments.

One problem with instrument attachment was the lack of an obvious place to wrap the string around the instrument itself without it shifting or coming undone during flight. With strong winds, the kite line is also incredibly taut. Furthermore, knots significantly reduce the tensile strength in the line and would be nearly impossible to do and undo without causing issues to the reel. Knots would also be bad for the string itself. At knot locations, the tensile force is exerted partially against the width of the string, rather than being spread out along the length. These knotted sections cannot withstand nearly as much force before breaking.

A simple solution was found. Once the kite is flying, the tension from the lifting force makes the string taut. The taut kite string can be wrapped around a series of lightweight metal carabiners, using the tension to secure them in place. The carabiners consist of a flat metal hook portion with a spring-loaded "gate" that can be opened and closed. The kite is first flown, the carabiner is opened, and the taut kite string is wrapped around the inside metal spine portion (Figure 9). Then, it is only a matter of attaching the instruments to the carabiners themselves, which is done after attaching the carabiner to the line.

Figure 9. A photograph depicting the placement of the carabiners on the kite string. The string is wrapped around the solid metal spine of the carabiner and the string tension holds the carabiners in place. Instruments are then attached to the carabiners to avoid using knots in the string.

The smaller iMet-XQs can be attached either to a single carabiner or to two carabiners. With one carabiner, the XQ is secured parallel against the flat spine with zip tie fasteners reinforced with duct tape before attaching the carabiner to the line (Figure 10). The duct tape keeps the XQ from slipping vertically. The larger iMet-XQ2 is attached to two adjacent carabiners, with the

flat portion positioned perpendicular against both carabiners in the middle. It is secured with two hook-and-loop fastener straps oriented horizontally and vertically along the instrument length to prevent it from slipping each direction. It can then be doubly secured with a zip tie fastener (Figure 11). The iMet-XQ can also be secured in the same way between two carabiners, using duct tape rather than straps. These methods of attaching the instruments to the string have proven to be quick, simple, and effective.

Figure 10. A photograph of an iMet-XQ attached to a single carabiner. The instrument is first attached to the carabiner, and then the line is wrapped around the instrument and the carabiner together to keep it in place during flight.

Figure 11. A photograph of the iMet-XQ2 attached to two carabiners on the kite string. First the carabiners are attached as in Figure 9, then a horizontal and vertical Velcro loop attach the instrument to the carabiner, and a zip tie further reinforces the attachment point.

2.4 Flight Locations

Most of our flights took place at Kaupō Beach (yellow star), located on the windward coast of southeast Oʻahu at 21.315343°N, 157.662237°W (Figure 12). It is an advantageous location for this study because it provides steady, uninterrupted winds coming perpendicularly onshore to the coastline during normal trade wind days (E-NE). We had normal trade wind days during roughly 66% of our flights. Most of our successful kite flights took place here, and it is a convenient setup spot with easy parking and a picnic table for instrument attachment. In addition, it is free from troublesome vegetation (cacti, as well as thorny and high bushes), which made kite

retrieval extremely difficult during early flights at other test locations including the top of nearby Makapu'u for example. A disadvantage of this location is that winds may be turbulent when they veer more northerly because two small islands, Mānana and Kāohikaipu, lay just off the coast to the north-northeast. Mānana Island, the larger of the two, is located 1.21 km from Kaupō Beach. It extends 707 m long and 654 m wide. It rises up to 110 m and thus may disturb the incoming low-level trade winds, making it difficult to launch the kite initially. Kāohikaipu is a low islet that lies directly south of Mānana Island, but it is comparatively very shallow. On turbulent days, we move south to Sandy Beach Park field (red star), because it provides ample room for setup and flying, and winds are generally steady here as well. However, a disadvantage is that winds are not always straight off the coast unless they are directly easterly-southeasterly. Issues dependent on the flight location and wind direction will be discussed in the Chapter 3 Results Section.

a.)

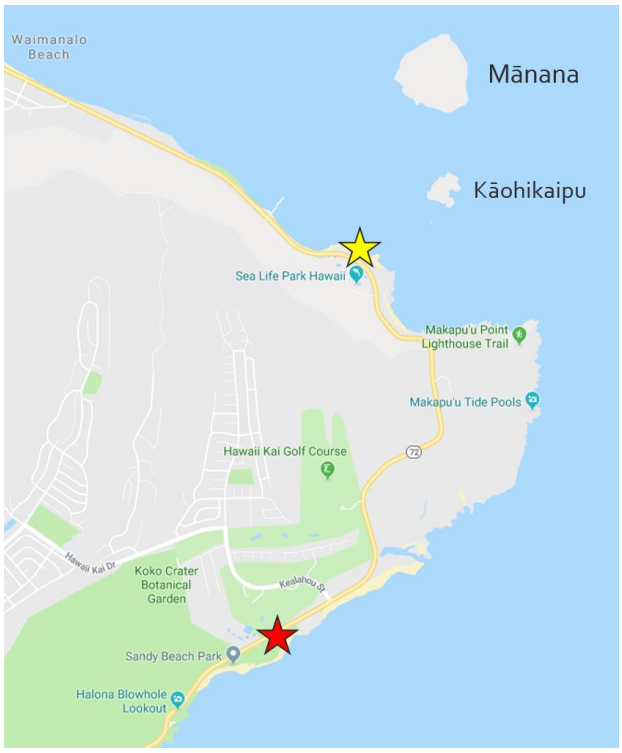

b.)

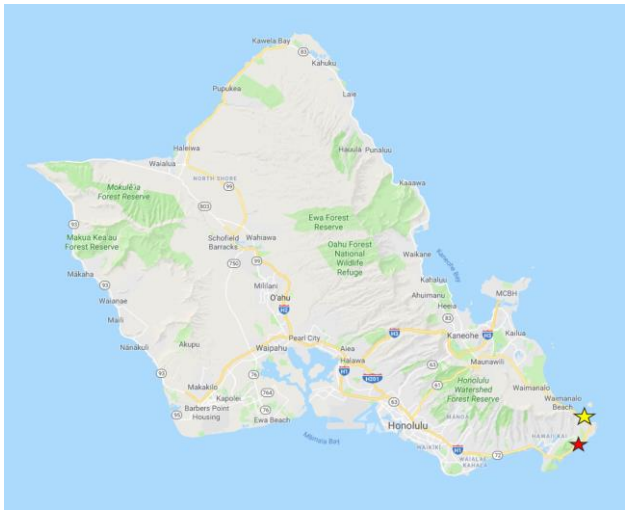

Figure 12. Adapted from Google Maps. a.) A map depicting a portion of the southeast corner of Oʻahu, Hawaiʻi. The two primary kite flying locations, Kaupō Beach and Sandy Beach, are indicated by the yellow and red stars, respectively. Mānana Island and Kāohikaipu are labelled. b.) A full map of Oʻahu, Hawaiʻi, with kite locations marked as above.

2.5 Data Collection

Before data can be collected, the winds must be tested to determine the size of delta conyne kite that will be flown. Kites with larger surface area generate more lift than smaller kites in the same wind conditions, so the size is chosen according to wind strength. Getting the kite off the ground typically requires two people: one to hold and loft the kite, and one to hold and control the electric fishing reel. Once the kite catches a gust of wind and is in the air, the slack in the line must be quickly tightened to increase the string angle, sending the kite up to a higher level where it will catch higher winds and be lofted further. More slack is then added gradually to allow the kite to gain additional altitude. If a certain height level is desired, the electric reel displays the amount of kite string that is deployed on-screen, so the amount of string can be controlled through manual stop and release.

The kite is flown alone for several minutes and at multiple altitudes to test the wind turbulence at various heights to make sure it is safe for taking measurements. On some flight days, the lower atmospheric boundary layer is too turbulent for observing, and the flight mission must be cancelled for the day. When the kite flies steadily, the kite is reeled in until it reaches the lowest possible stable height to attach the first sensor. Turbulence is greater close to the surface, and the optimal stable kite flying height is typically found with the line extended between 25-75 m. We attach sensors as close to the kite as possible, so that when the line is extended it can take measurements of air as high as possible above the surface-modified layer of the atmosphere. During most flights, an iMet-XQ2 was attached first, because it has the greatest accuracy and battery life. The kite is typically stable when approximately 50 m of line is deployed, corresponding to the first instrument being attached approximately 40-45 m below the altitude of the kite with an average string angle of 60°. After the first sensor is attached, additional sensors

are attached lower down the string at intervals of 50 or 100 m, which is measured by the electric fishing reel (Figure 13). This is done until the line is fully extended to approximately 600 m. In order to observe variations in temperature and humidity at a constant altitude, the kite is maintained at a constant string length for time periods of around 30 minutes. Constant altitude flights of one hour or more are preferred, however, and are used whenever possible.

Figure 13. A photograph looking upwards of a delta conyne kite flying with three sensors attached to the kite string, separated at 50 m intervals.

2.5.1 Temperature Correction

Although keeping the string length constant helps the kite to maintain a relatively constant altitude, turbulence causes random upward and downward movements to occur. The vertical movements cause variations in the recorded atmospheric variables, because they typically all vary with altitude. However, we are concerned with perturbations in temperature and humidity at a constant altitude independent of vertical variations. In order to account for vertical movement of the kite, we correct the observed temperature to a constant altitude, assuming that our measurements take place in the well-mixed boundary layer with a dry adiabatic lapse rate. In the following section you will see that this is well justified. We use the following formula to correct the observed temperature to a constant altitude:

$$T_z = T + \frac{g}{C_{pd}} dz, \text{ (Eqn. 1)}$$

where T_z is the altitude-corrected temperature, T is the recorded air temperature, g is the gravitational acceleration constant equal to -9.8 m s^{-2}, C_{pd} is the specific heat capacity of dry air at constant pressure ($C_{pd} \approx 1004$ J K^{-1} kg^{-1}), and *dz* is the deviation in altitude from the mean along the constant altitude portion in meters:

$$dz = z - \bar{z} \text{ (Eqn. 2)}$$

Specific humidity is assumed to have negligible variance from small changes in altitude. An example of altitude-corrected temperature is given in Figure 14.

a.)

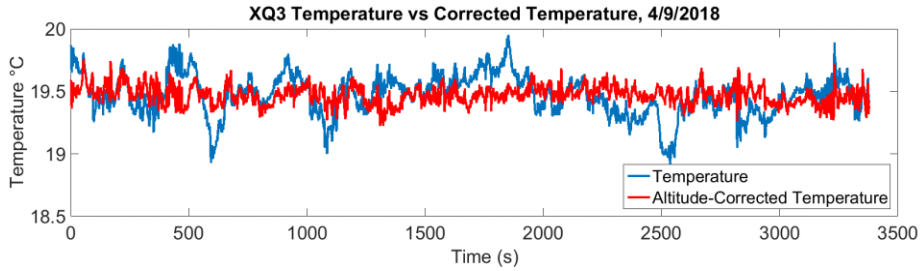

b.)

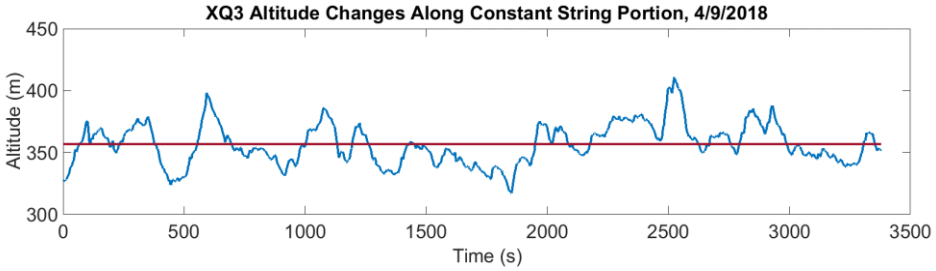

Figure 14. a.) Temperature (°C, blue) observed by the iMet-XQ2 instrument and temperature (°C, red) corrected for vertical variations on the scale of 50 m during the constant altitude portion of Flight 9. b.) Altitude (m, blue) along the constant string portion over time (s), compared to a mean constant altitude of 356.7 m.

2.6 Flight Data

Table 2 summarizes the data collected from all successful flight days, where instruments were lofted via kite and observations were collected. Note that there were multiple unsuccessful flight days where a test flight was flown, but data was not collected due to unfavorable winds, strong turbulence, or equipment failure. These days are not included in Table 2. The date, flight start time, and flight length in minutes are included, as well as the flight location. All but two successful flight days took place at Kaupō Beach. The specific instruments deployed during each flight are listed, and numbered based on the order they were acquired. XQs numbered 1, 2, 4, and

5 denote the original iMet-XQ version, while XQs numbered 3, 6, 7, 8, 9, and 10 denote the upgraded iMet-XQ2 sensors. The length of kite string let out is the maximum length of string deployed during the flight, and is limited by the amount of line on the electric reel. The maximum deployed line decreased after the first few flights due to instances where it needed to be cut. Typically, after this maximum string length is deployed, it is kept constant for the purposes of observing incoming temperature and humidity variations at a quasi-steady altitude. The maximum altitude of the highest-attached sensor is also listed. This differs from the maximum deployed string length due to the string angle, curvature of the line, and sensor distance from the kite. The mean surface wind information is also provided for each day, measured with a hand-held kestrel at the launch location.

Most flights occurred in Fall 2017 and Winter 2017/18. During the first few flights (September – November 2017), only one or two iMet-XQs were attached to the string. These reached maximum altitudes between roughly 400-610 m. Later, additional iMet-XQs were acquired, as well as one upgraded iMetXQ2. Three to five of these instruments were attached to the string during Flights 5-8, (Winter 2017/18). The more accurate iMet-XQ2 was always attached closest to the kite when possible. Additional iMet-XQ2s were acquired during Spring 2018. Five iMet-XQ2s were attached to the kite string during Flight 9, while one iMet-XQ2 took surface measurements. This appears to be the most ideal setup thus far, which could be improved by the acquisition and deployment of additional iMet-XQ2s. During Flights 5-9, maximum altitudes of 380-520 m were reached, due to a decrease in the amount of line wound on the reel. The length of string on the reel primarily determines the maximum altitude for each flight.

Figure 15 helps to illustrate the sampling technique used in each flight by showing the altitude of the highest-attached sensor with time. For example, in Flight 1 (Figure 15 top left),

the kite was kept steady at multiple string lengths (300 m, then surface, then 450 m, 600 m, 750 m, and 800 m) as it ascended before being brought back down to the surface. This corresponds respectively to altitudes of roughly 260 m, 365 m, 460 m, 560 m, and 605 m for all constant string lengths above the surface. Flights 2, 4, 5, 6, 7, 8, 9 each show a clear constant altitude portion. The winds had greater turbulence on several days, as seen in the large vertical movements of Flights 2 and 4. On other days, the winds were steadier, as indicated by the relatively flat constant altitude portions of Flight 5, 6, and 8. Flight 6 shows a halt in the data collection where the kite entered a cloud deck immediately prior to descent, causing the highest attached instrument to malfunction. Each flight differs depending on the conditions experienced, the sampling strategy which sometimes depended on the conditions, and on the instrumentation and line length available. Figure 16 provides an example of time series plots of the altitude of multiple iMetXQ2 sensors attached to the same string during Flight 9. In this plot, temperature variations can be seen along the string compared to the surface temperature over time. During this particular flight, the sun set behind the mountains toward the end of the data set, causing the observed decrease in surface temperature.

2.6.1 Data Selection

For a short time period (<5 minutes) immediately after the instruments are turned on, there are large inaccuracies in the GPS sensor data. This is due to the time required for the sensors to acquire a signal from a sufficient number of GPS satellites. So far, it has been found that the GPS-related quantities (latitude, longitude, altitude, time) have large inaccuracies for a satellite count less than 5. Generally, it takes under 5 minutes for the iMet-XQ to connect to a minimum of 5 GPS satellites. This time is typically much shorter for the iMet-XQ2 (~1 min), which has a more accurate GPS sensor due to a larger copper plate, which accounts for its increased size. On

some days, it may take up to 15 minutes for GPS to fully connect. Due to the above information, data is only considered usable when the iMet-XQ SatCount ≥ 5. In addition, only GPS altitudes > 0 m are used, in order to account for any additional unusual GPS errors.

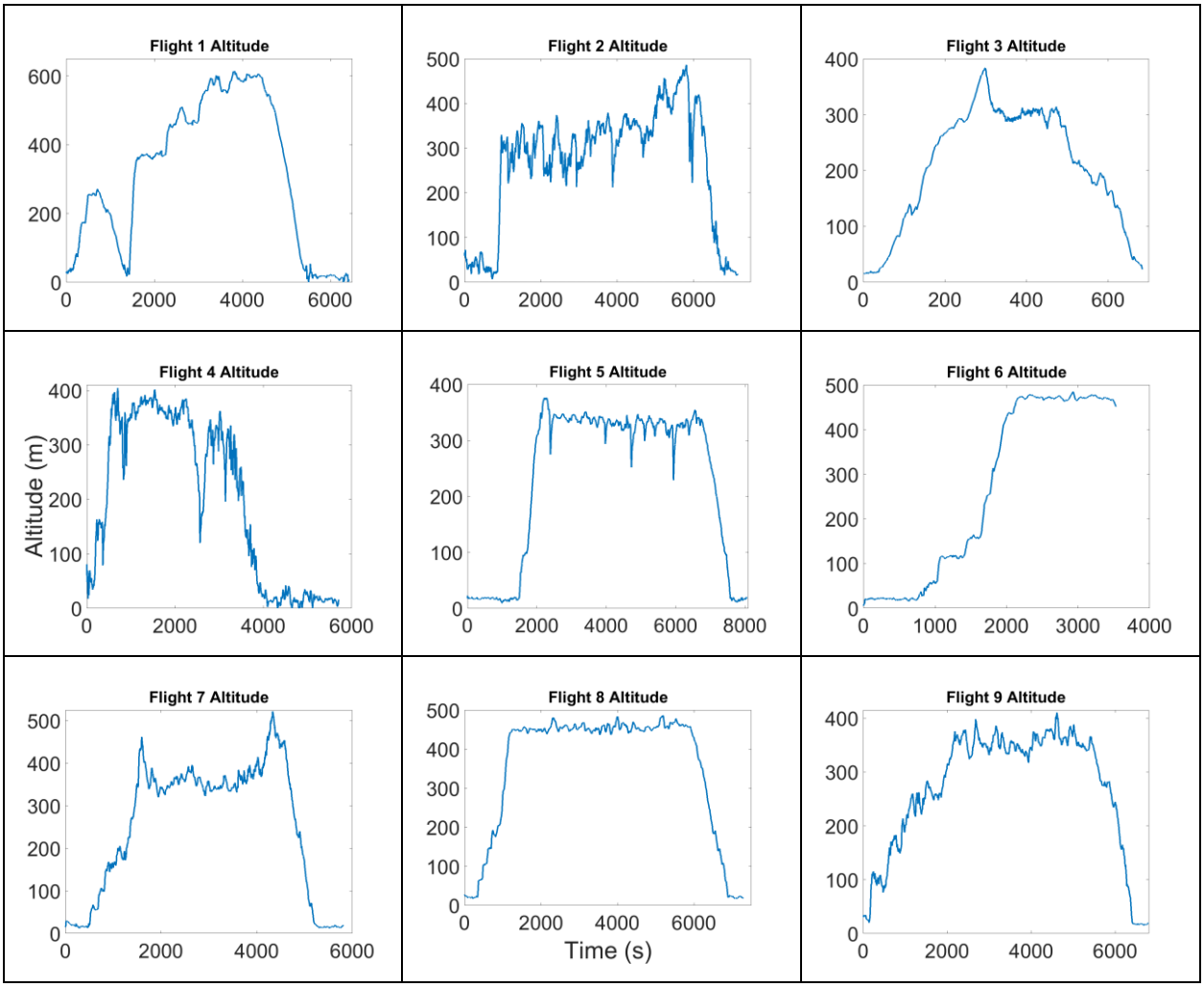

Figure 15. Time series plots (s) of the altitude (m) of the highest attached sensor for each of the nine flights. On flights 1, 2, 3, and 4, the top sensor was an iMet-XQ sensor while on flights 5, 6, 7, 8, and 9, the top sensor was an iMet-XQ2 sensor with higher accuracy. Flight 3 (top, right) was particularly short due to turbulent conditions. Flight 6 (middle, right) cuts off short during flight due to a cloud moisture-related sensor error.

Table 2. Overview of data from all successful kite flight days. The table includes date, time, duration, location, instruments used, wind and altitude information. KB refers to the Kaupō Beach location, and SB refers to the Sandy's Beach field location.

Flight Number	1	2	3	4	5	6	7	8	9
Date	9/21/17	10/5/17	10/20/17	11/24/17	1/25/18	2/22/18	3/9/18	3/22/18	4/9/18
Flight Start Time (HST)	3:15 PM	2:45 PM	4:00 PM	1:00 PM	9:15 AM	9:50 AM	3:25 PM	10:30 AM	4:50 PM
Flight Length (mins)	90	105	15	70	105	60	80	105	105
Flight Location	KB	KB	KB	KB	KB	KB	SB	KB	SB
Instruments Used	1	1	1, 2	1, 2	1,2,3	1,3,4,5	1,2,3,4,5	1,2,3,4,5	3,6,7,8,9,10
Length of Kite String Let Out (m)	800	750	450	525	550	550	615	625	600
Maximum Altitude Measured (m)	610	490	400	400	380	480	520	490	410
Average Surface Wind Speed (m/s)	4	5	4	4.5	3	2	4.5	4	3
Average Surface Wind Direction	E	E	E	NE	ESE	ESE	NE	ESE	NE

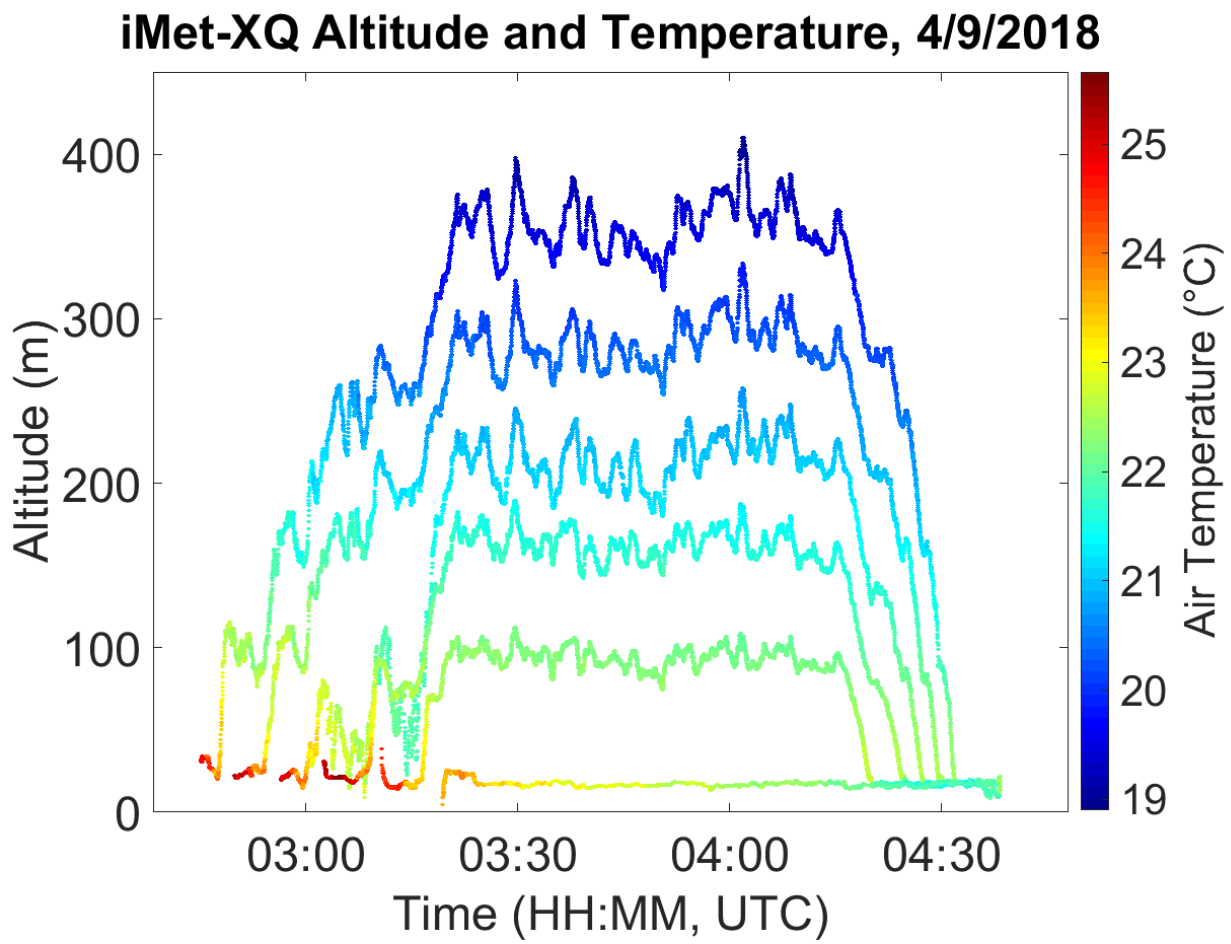

Figure 16. Time series plot of the iMet-XQ2 altitude of all sensors during Flight 9 (HH:MM in UTC time), colored according to temperature (°C). From the top, sensors were attached in this order: #3, 7, 6, 8, 9. XQ#10 took surface measurements. A marked decrease in surface temperature can be seen from the beginning of the flight to the end, following sunset.

CHAPTER 3: RESULTS

The techniques outlined in the prior chapters are applied to the collected datasets in order to make insights about the marine boundary layer. In previous sections, we showed how we were able to successfully develop a low-cost kite observation platform, including the necessary skills and tools to do so, and use the kite platform to take measurements of the incoming low level trade winds within the marine boundary layer. In this section, we will look for evidence of moist "seeds" of convection in the collected datasets. In order to do so, we will:

1) Build confidence in the collected datasets by verifying expected atmospheric patterns.
2) Isolate the constant altitude portions of the kite datasets, and examine variations in temperature and specific humidity perturbations in these portions.
3) Examine the correlation between constant-altitude temperature and humidity perturbations in the low-level marine boundary layer trade winds.

3.1 Verifying Expected Patterns

In order to build confidence in the accuracy of the sensor observations, we verify some patterns that we would expect to see in the well-mixed boundary layer region. The potential temperature, θ, is the temperature that an unsaturated air parcel would have if it were brought down dry adiabatically to a standard pressure level, p_0, usually 1000 hPa. It is given by the following equation:

$$\theta = T(\frac{p_0}{p})^{\frac{R_d}{C_{pd}}}. \text{ (Eqn. 3)}$$

The symbol θ is potential temperature (K), T is the air temperature (K), p is the pressure of the parcel (Pa), R_d is the gas constant for dry air (287 J K^{-1} kg^{-1}), and C_{pd} is the specific heat capacity

of dry air at constant pressure (1004 J K^{-1} kg^{-1}). R_d/C_{pd} is a constant roughly equal to 0.286. Until a rising parcel of air is saturated, it cools at the dry adiabatic lapse rate, -9.8°C km^{-1}. Assuming our measurements are in the well-mixed marine boundary layer, we should expect the environmental lapse rate below the LCL to be dry adiabatic, and θ should be constant with altitude, because θ is conserved for dry adiabatic ascent. Figure 17a shows a plot of observed temperature with altitude of the highest sensor for each flight day against a reference dry adiabatic lapse rate line. The potential temperature of the highest sensor is plotted in Figure 17b with altitude across all flights. The expected dry-adiabatic lapse rate temperature change and constant θ with altitude is observed, and the temperature variations between each flight day appears to be primarily due to the seasonal temperature changes. We can thus assume that the sampled atmosphere is well-mixed.

To further verify expected relationships, the altitude of the attached sensors may be acquired in two ways. The iMet-XQ and iMet-XQ2 sensors are equipped with a GPS sensor that provides altitude information, and altitude can also be derived from the observed atmospheric pressure. These values should be similar to one another if the GPS and pressure sensors are reliable. The altitude can be derived from the pressure by utilizing the hypsometric equation:

$$z_2 = \frac{R_d \bar{T}_v}{g} \ln\left(\frac{p_1}{p_2}\right) + z_1. \text{ (Eqn. 4)}$$

Z_2 is the pressure-calculated altitude, Z_1 is the height of the surface above sea level, $\bar{T}_v$ is the layer-mean virtual temperature, p_1 is the atmospheric pressure at Z_1, and p_2 is the sensor pressure, which is used to derive Z_2. $\bar{T}_v$ is calculated as the mean temperature across the entire dataset, because the layer that the kite flies in is relatively shallow. Z_1 is taken as the minimum GPS altitude in the dataset, which is typically 15-17 m above sea-level at Kaupō Beach. The

minimum altitude in a given dataset is sometimes unusually low due to GPS inaccuracies shortly after the device is turned on. In these cases, a value of 16.9 m is used for Z_1. This value is taken from the surface GPS altitude from a reliable iMet-XQ2 dataset at Kaupō Beach. Figure 18 gives comparisons of the GPS altitude with the pressure-derived altitude from example flights using an iMet-XQ and an iMet-XQ2. In both Figure 18a and 18b, the GPS altitude is extremely close to the pressure-derived altitude. An average difference of only 9.85 m and 1.01 m are found in these two typical sample datasets. The error is larger with the less accurate iMet-XQ instrument as compared to the improved iMet-XQ2 instrument.

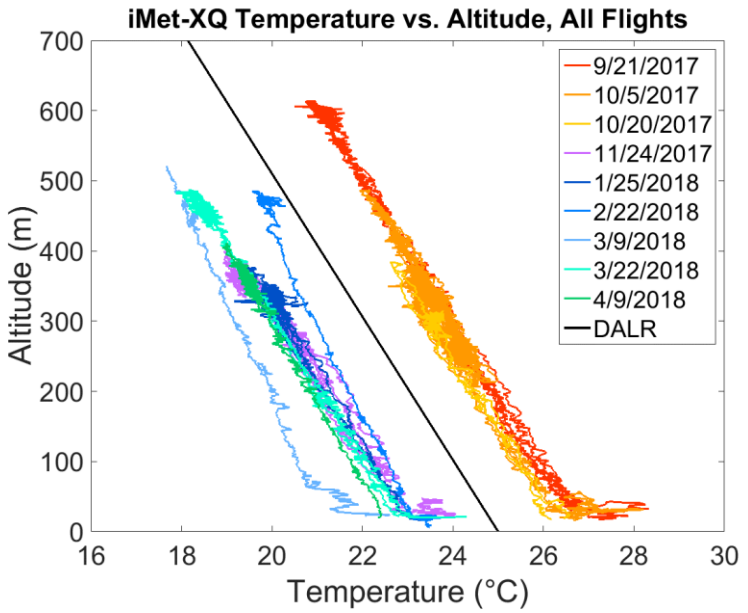

a.)

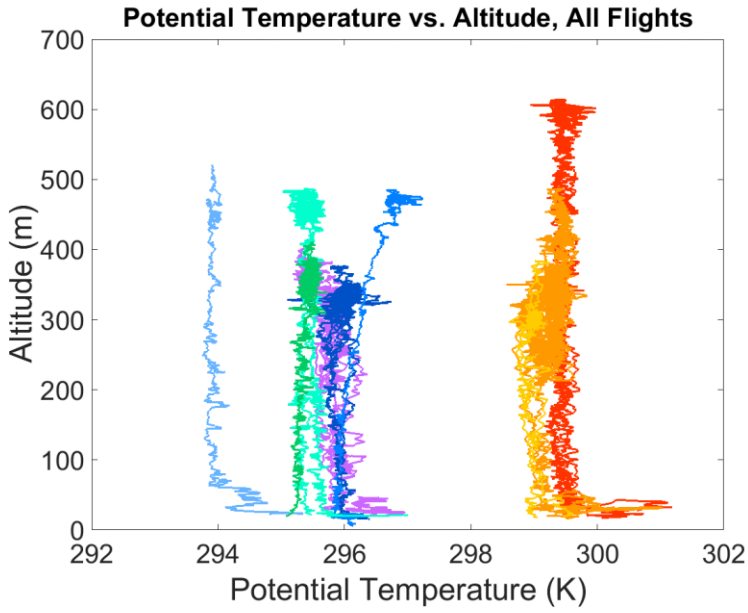

b.)

Figure 17. a.) Air temperature (°C) with altitude (m) for all flight days. Data is collected using the highest attached sensor for each day. The black reference line shows the dry adiabatic lapse rate of -9.8 °C/km. Individual flights are color-coded by date, which is provided in the legend. Flights in summer months are colored with warm colors. b.) Same as above, but for potential temperature (K).

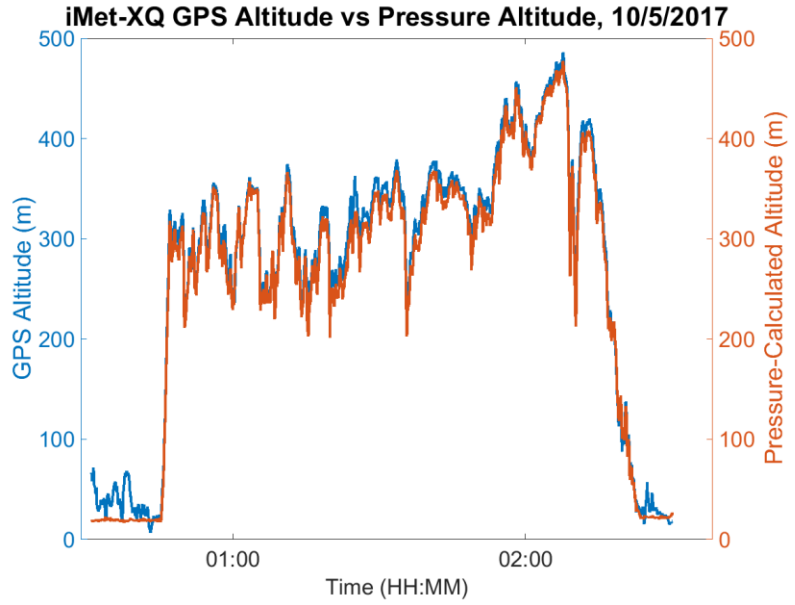

a.)

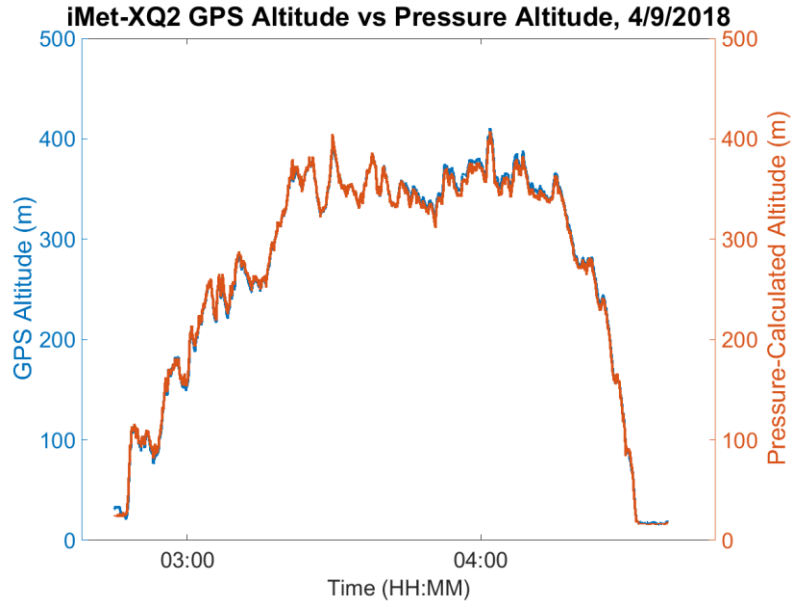

b.)

Figure 18. a.) A time series comparison of the iMet-XQ GPS-observed altitude (blue, solid, m) and the pressure-derived altitude (orange, solid, m) over time from Flight 2. b.) The same as above, except data is collected using an iMet-XQ2, from Flight 9.

3.2 Temperature and Humidity Perturbations at Constant Altitude

As discussed in Chapter 1, strongly anticorrelated patches of cool, moist air and warm, dry air were observed in-situ by aircraft in the steady trade wind flow upstream of Dominica during the DOMEX field campaign at an altitude of 300 meters. The moist patches, or "seeds" of convection in particular are theorized to be important for convective initiation as the entire layer is uniformly lifted over the higher terrain of the island. The current study seeks to learn whether the same anticorrelated T_z and q_v perturbations can be observed in the trade wind flow upstream of O'ahu by taking measurements at a steady altitude along the windward coast above the surface layer, where observations may be characteristic of the upstream environment. During most flights, sensors were flown at a constant altitude above 300 m for time periods of at least 30 minutes (except for Flight 3). T_z and q_v variations are examined during these constant altitude portions for the purpose of observing moist "seeds" of convection. The constant altitude portions of each flight are not immediately identifiable in the data due to random upward and downward motions of the kite. The constant altitude segments are therefore identified by isolating the durations of time where the kite string length is held constant. The kite string length is approximated as the hypotenuse of a triangle created by two legs formed by the horizontal and vertical distance between the sensor, a point on the ground directly below the sensor, and the kite reel launch location (Figure 19). Once the constant string length portion is identified, then temperature is corrected within this portion (T_z) for the random vertical motions in the kite string, assuming a dry adiabatic lapse rate of a well-mixed boundary layer atmosphere. This same correction is used in NS14 to correct for changes in aircraft flight altitude.

a.)

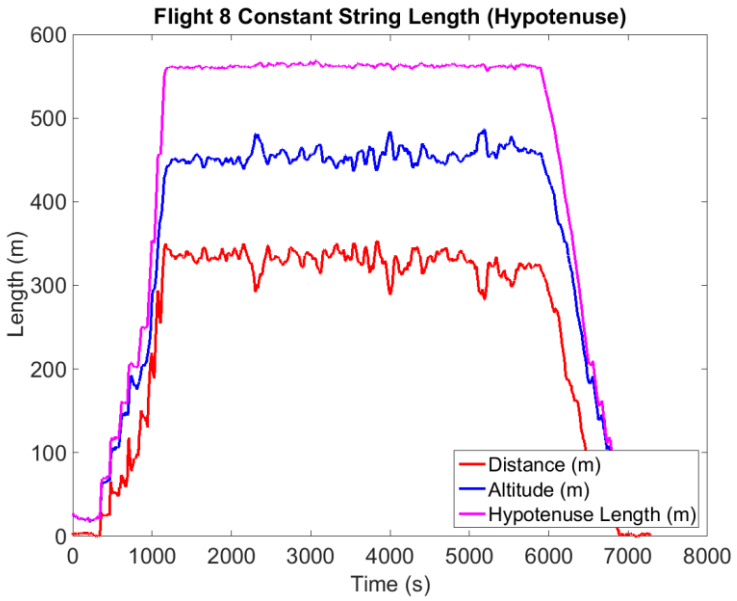

b.)

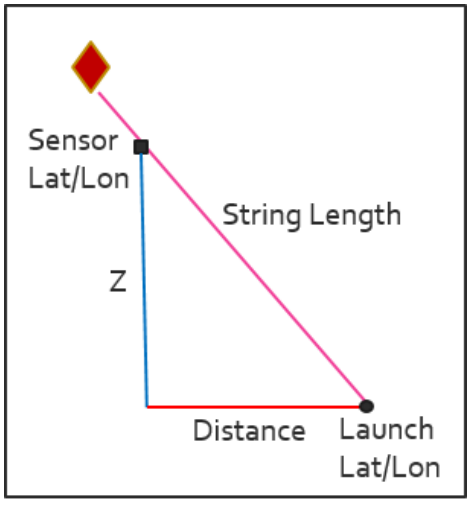

Figure 19. a.) Schematic illustrating the relationship between the string length (pink, solid), the horizontal distance between the sensor and the reel (red, solid), and the altitude of the sensor (blue, solid) during Flight 8. b.) A simple diagram showing the three legs of the triangle formed between the sensor, the ground, and the kite launch point. The string length is approximated as the hypotenuse (pink, solid). The red diamond shape represents the kite itself.

The raw T_z (°C) and q_v (g kg^{-1}) perturbations (T_z', q_v') during the constant altitude portion of Flight 8 are shown in Figure 20 as an example. The values are calculated by subtracting the mean values of T_z and q_v along the constant altitude portion from the observed values. T_z' and q_v' are then plotted against each other. Flight 8 is chosen as an initial example case because of its relatively long duration (~80 mins) constant altitude flight portion at ~450 m, on a day where the trade winds were steady. T_z' and q_v' are smoothed using a moving average filter with a span of 100 data points. The moving average filter operates on the dataset by averaging a number of points from the input measurement in order to produce the output. The input measurement acts as the center of the averaged data. For example, if a moving average filter with a span of 5 were used, the output would be the average of 2 data points behind the input, the input itself, and 2 data points in front of the input. This averages 5 data points total before moving on to the next input. In the examples below, 100 data points are averaged around each input measurement. This acts as a low-pass filter and removes the high frequency variations in each dataset.

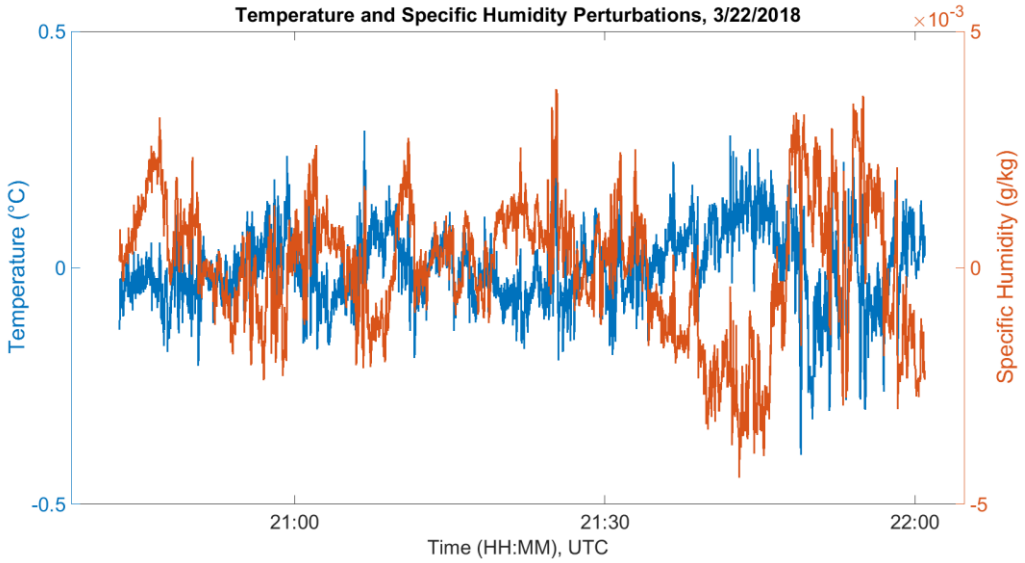

a.)

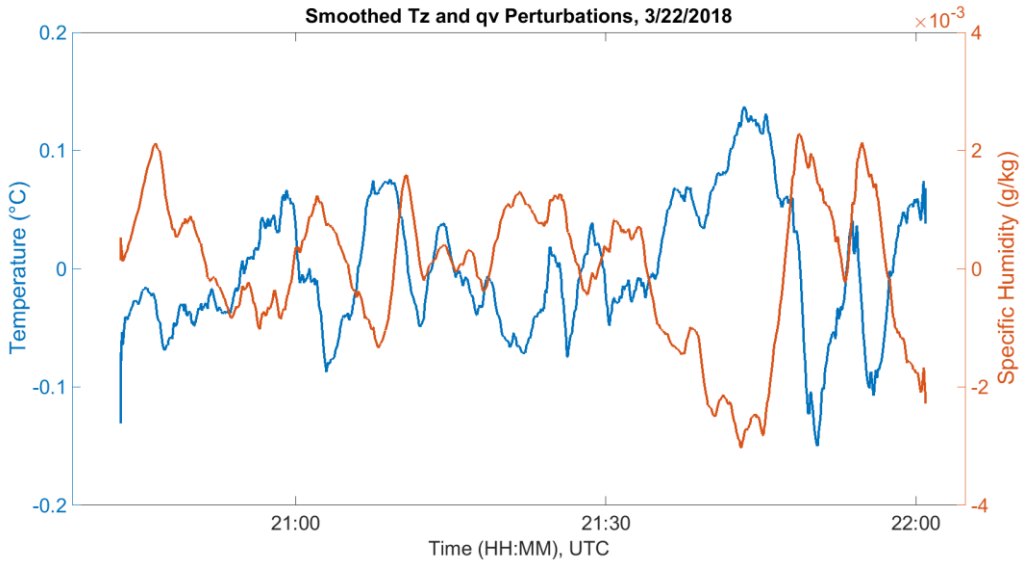

b.)

Figure 20. a.) The unsmoothed altitude-corrected temperature (blue) and specific humidity (orange) perturbations (T_z', q_v') along the constant altitude portion of Flight 8, at 456 m. Correlation coefficient is -0.1648. b.) Same as above, but smoothed using a moving average filter with a span of 100 data points. The correlation coefficient of the smoothed curves is -0.7679.

T_z' and q_v' become more strongly anticorrelated when the high-frequency variations in the dataset are smoothed out. This is further discussed in Chapter 4. T_z' and q_v' are also found to be anticorrelated in the constant altitude segments of Flights 1, 2, and 4. In these cases, the correlation coefficient between T_z' and q_v' becomes increasingly negative when the data is smoothed as before. The unsmoothed and smoothed perturbations for these flights are shown below (Figures 21, 22, 23). A moving average filter with a span of 100 data points is used on the datasets as before.

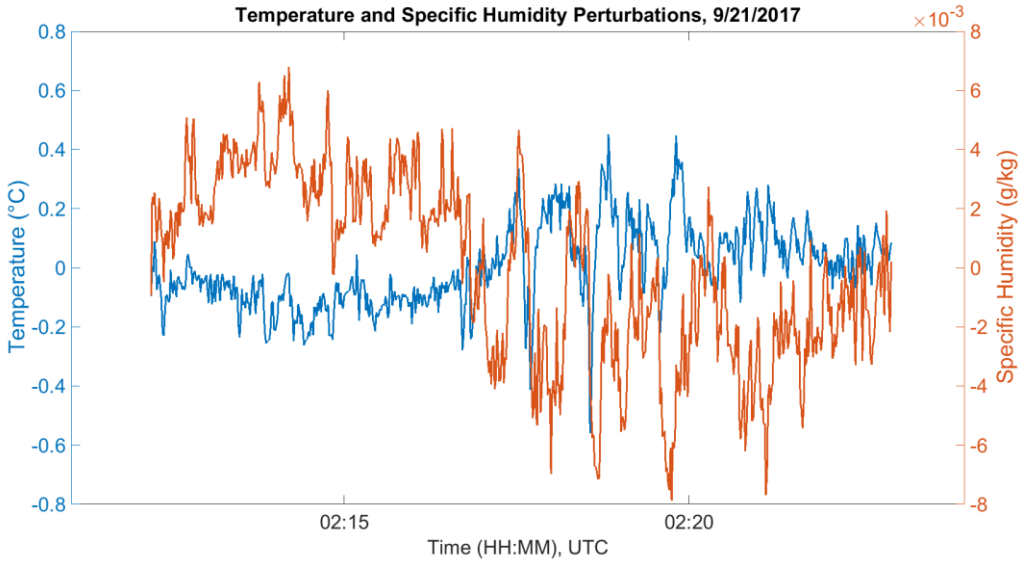

a.)

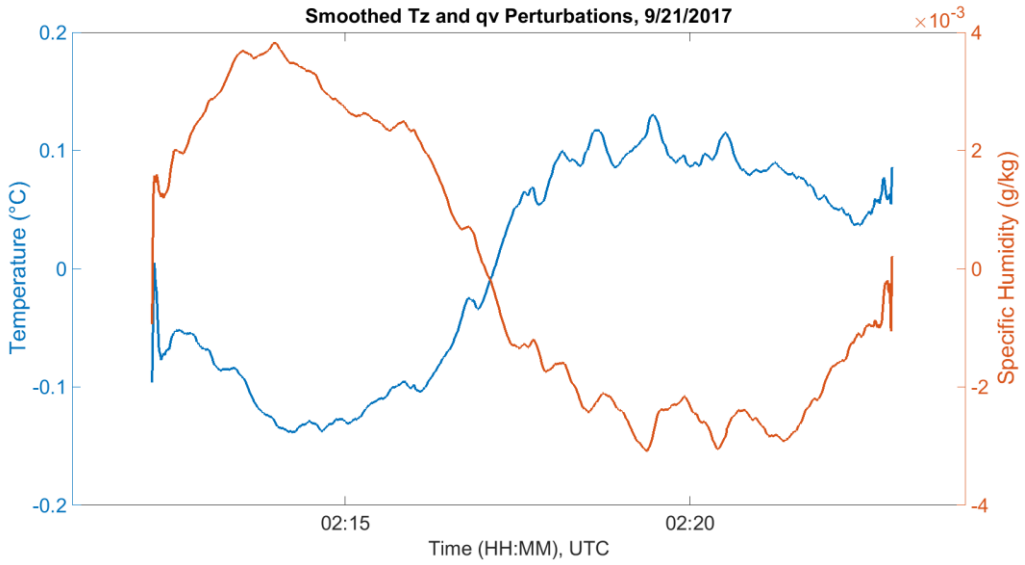

b.)

Figure 21. a.) The unsmoothed altitude-corrected temperature (blue) and specific humidity (orange) perturbations (T_z', q_v') along the constant altitude portion of Flight 1, at 596 m. Correlation coefficient is -0.4763. b.) Same as above, but smoothed using a moving average filter with a span of 100 data points. The correlation coefficient of the smoothed curves is -0.9716.

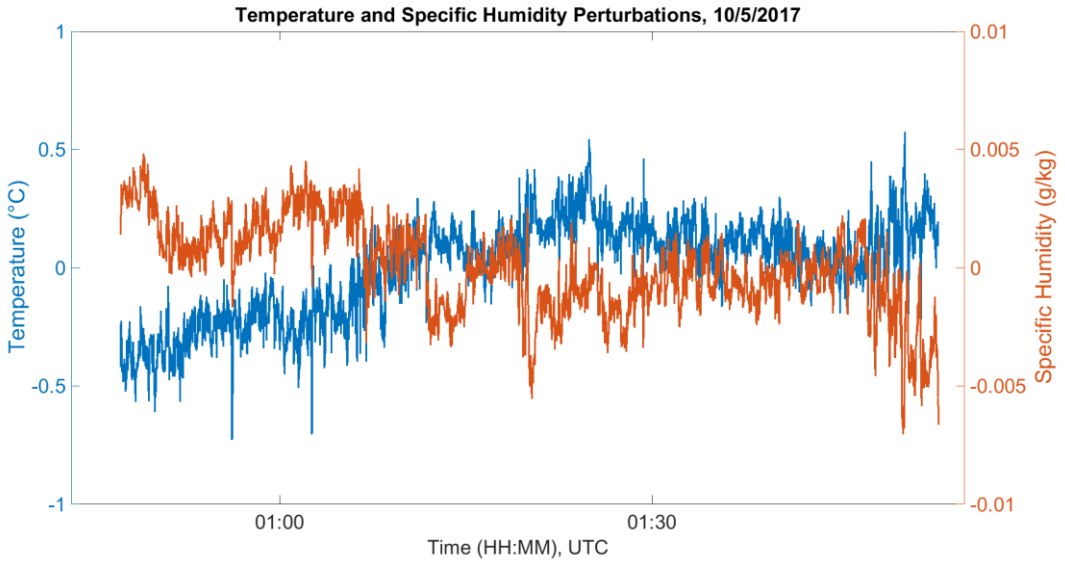

a.)

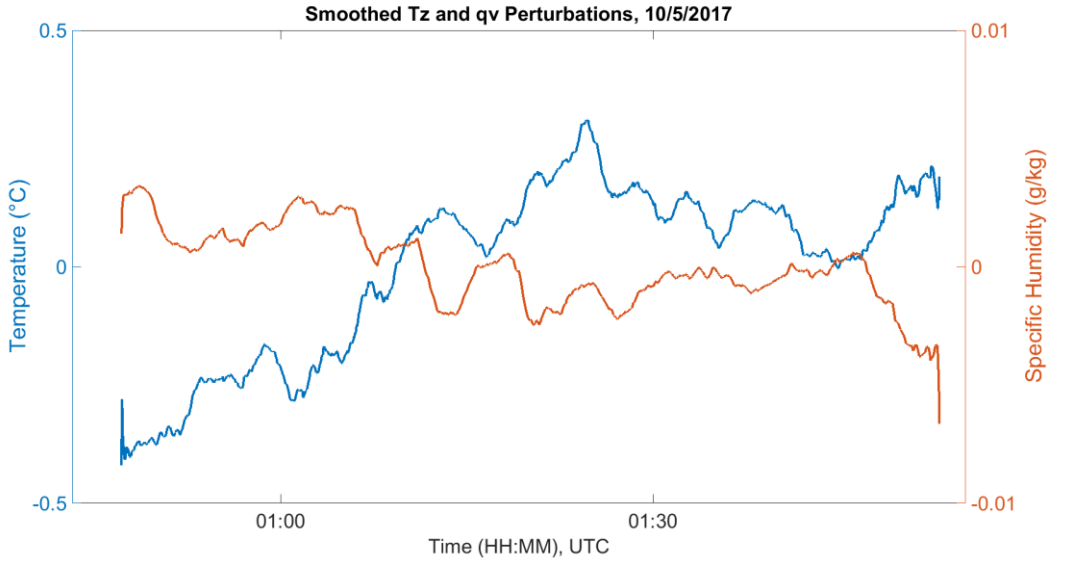

b.)

Figure 22. a.) The unsmoothed altitude-corrected temperature (blue) and specific humidity (orange) perturbations (T_z', q_v') along the constant altitude portion of Flight 2, at 334 m. Correlation coefficient is -0.6205. b.) Same as above, but smoothed using a moving average filter with a span of 100 data points. The correlation coefficient of the smoothed curves is -0.8402.

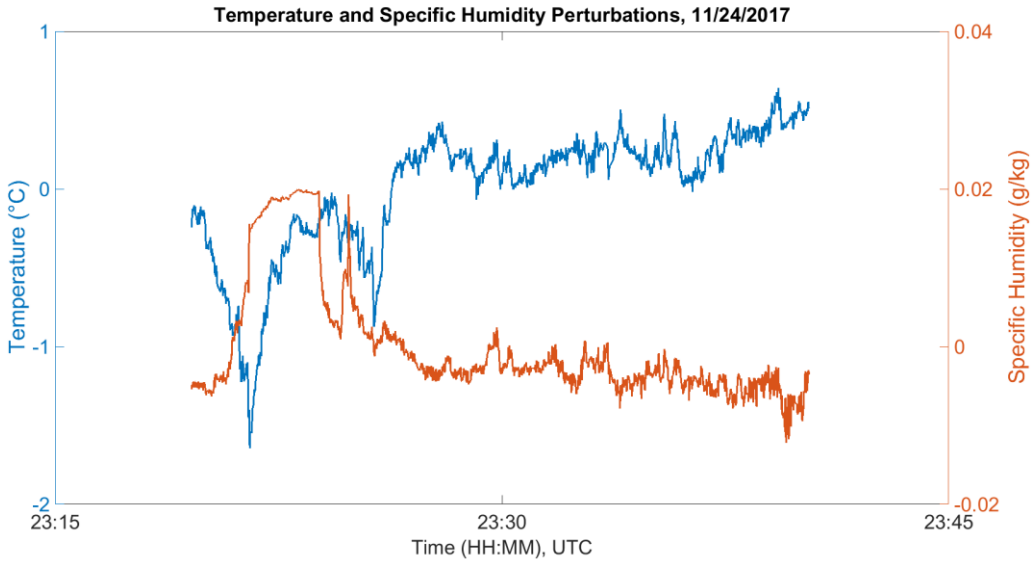

a.)

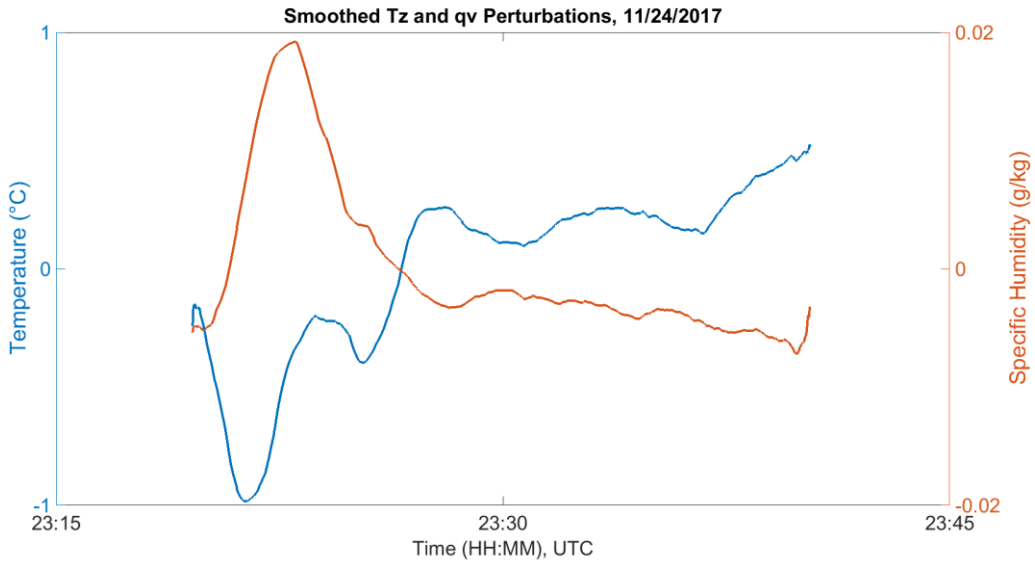

b.)

Figure 23. a.) The unsmoothed altitude-corrected temperature (blue) and specific humidity (orange) perturbations (T_z', q_v') along the constant altitude portion of Flight 4, at 368 m. Correlation coefficient is -0.6176. b.) Same as above, but smoothed using a moving average filter with a span of 100 data points. The correlation coefficient of the smoothed curves is -0.7174.

A strong anticorrelation between T_z' and q_v' is not found in every dataset. Below, T_z' and q_v' along the constant altitude portion of Flight 9 are plotted as an example where the correlation is weak and positive (Figure 24). Smoothing weakens the correlation, but does not cause it to become negative.

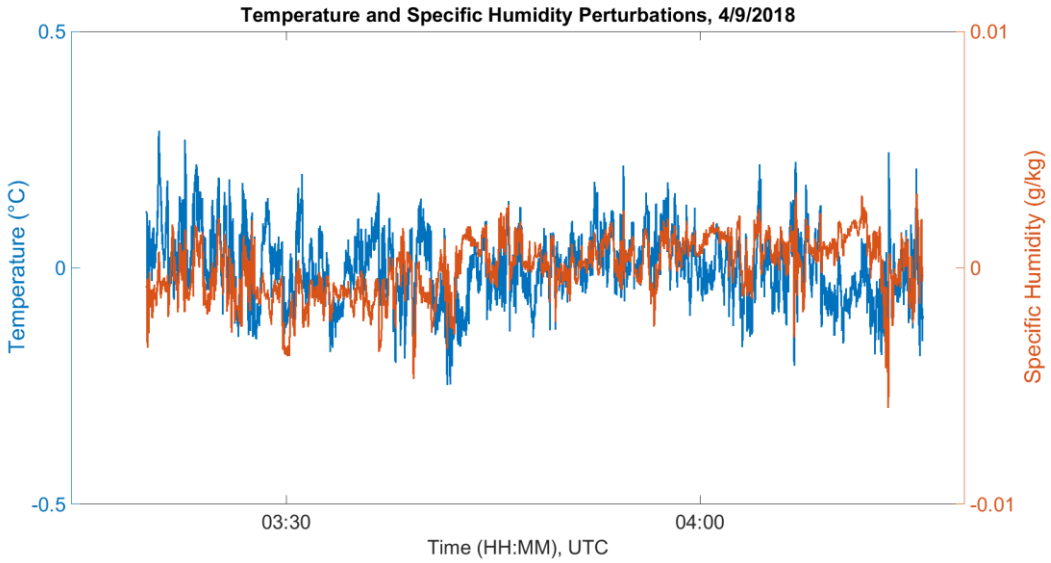

a.)

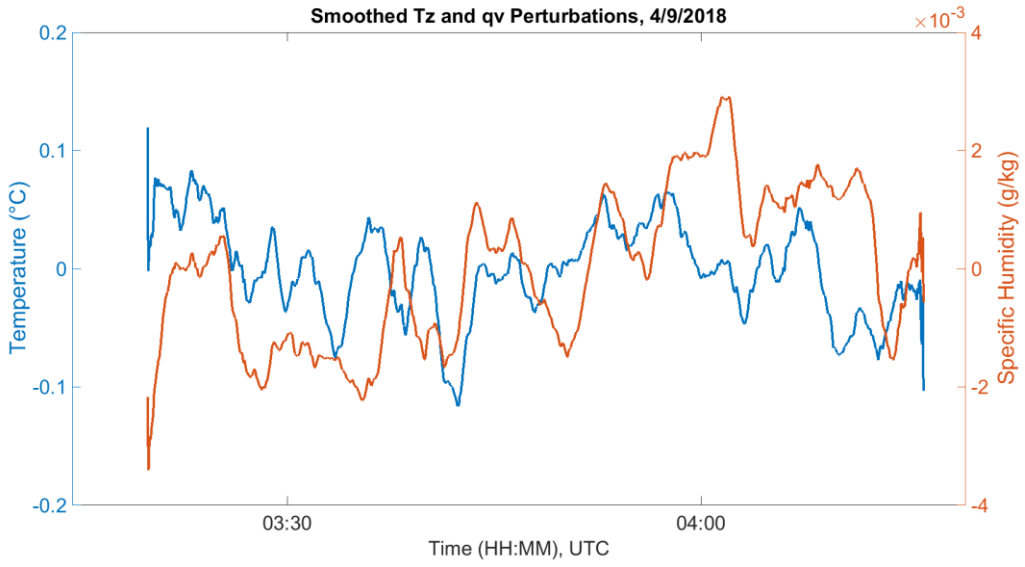

b.)

Figure 24. a.) The unsmoothed altitude-corrected temperature (blue) and specific humidity (orange) perturbations (T_z', q_v') along the constant altitude portion of Flight 9, at 357m. Correlation coefficient is 0.3889. b.) Same as above, but smoothed using a moving average filter with a span of 100 data points. The correlation coefficient of the smoothed curves is 0.1418.

The table below summarizes the correlations found between temperature and specific humidity perturbations along the constant altitude portions of all flights except Flight 3, which does not have a constant altitude portion. The mean altitude and time duration of each constant altitude portion is given. The correlation coefficient of the raw and smoothed datasets for each flight is also given. Smoothed datasets use a running mean filter with a span of 100 data points. The duration of each constant altitude portion is given to illustrate the relative amount of data being sampled in each flight.

Table 3. A summary of the mean altitude and duration of the constant altitude portions of each flight, as well as the correlation coefficients (CC) between corresponding perturbations of altitude-corrected temperature (T_z', °C) and specific humidity (q_v', g/kg). The correlation coefficients between the smoothed T_z' and q_v' datasets of each flight are also provided. Here, a running mean filter is used with a span of 100 data points.

Flight Number	Mean Constant Altitude (m)	Flight Time (mins)	T_z' Q_v' Raw CC	T_z' Q_v' Smoothed CC
1	596.49	10.77	-0.4763	-0.9716
2	334.04	65.97	-0.6205	-0.8402
4	368.3	20.68	-0.6176	-0.7174
5	332.27	76.52	0.1067	-0.0271
6	471.87	21.98	0.2763	0.1126
7	352.81	32.32	0.2539	0.1629
8	455.5467	78.33	-0.1648	-0.7679
9	356.71	56.33	0.3889	0.1418

Out of all flights where T_z' and q_v' were found to be anticorrelated, Flight 8 is the only instance where reliable data was collected by multiple instruments at different points along the kite string. This allows us to examine the strength of the anticorrelation at multiple altitudes, providing an estimate of the vertical extent of the anticorrelated moist and dry patches of air in the incoming flow. We examine the correlation coefficient between T_z' and q_v' along the constant altitude portions of the data collected by each instrument along the string. The table below provides the correlation coefficient between the raw T_z' and q_v' datasets at each mean altitude, as well as that of the smoothed datasets using a moving average filter with a span of 100 data points.

Table 4. The mean altitude of several instruments along the kite string during the constant altitude portion of Flight 8, as well as the correlation coefficients (CC) between corresponding perturbations of altitude-corrected temperature (T_z', °C) and specific humidity (q_v', g kg^{-1}). The correlation coefficients between the smoothed T_z' and q_v' datasets of each instrument are also provided. Here, a running mean filter is used with a span of 100 data points.

Mean Constant Altitude (m)	T_z' q_v' Raw CC	T_z' q_v' Smoothed CC
455.55	-0.1648	-0.7679
416.82	-0.4091	-0.7768
374.22	-0.0519	-0.4712
285.09	0.0572	0.0291

CHAPTER 4: DISCUSSION AND SUMMARY

4.1 Conclusions

During the course of this study, it is found that even today, kites are a viable platform for making high quality in-situ observations of the atmospheric boundary layer. Accurate meteorological sensors are able to be made smaller, and are capable of being easily fitted to a kite string without tying knots or weakening the tensile strength of the string. Using kites as a platform, long-duration flights are possible, and observation times are limited only by the battery life of the sensors. In addition, we are able to sample atmospheric properties throughout the boundary layer at multiple altitudes simultaneously, by attaching multiple sensors along the string at fixed lengths. In doing so, we can produce vertical profiles and time series datasets of temperature, relative humidity, pressure, and position, as well as other variables derived from the above. We are able to show the accuracy of the meteorological sensors used in this study by verifying several expected relationships in the mixed atmospheric boundary layer. In nearly all flights, the air temperature lapse rate is found to be dry adiabatic with altitude (Figure 17). This also gives us a constant potential temperature with altitude. In addition, we find that the altitude derived from GPS satellite measurements agrees well with the altitude derived from the sensor pressure using the hypsometric equation. The iMet-XQ2 has an improved GPS sensor from the iMet-XQ, and this is reflected in how well the GPS altitude agrees with the pressure altitude (Figure 18).

After confidence is reached in the accuracy of our sensors, we use our collected datasets to study temperature and humidity perturbations in the incoming trade wind flow off the windward coast of O‘ahu. T_z’ and q_v’ are anticorrelated in the constant altitude flight segment in roughly

half of our datasets, pointing to the possibility of using kites to observe moist "seeds" of convection as in Nugent and Smith (2014).

Flight 8 is presented as a good example case where temperature and humidity perturbations may be examined along a long-duration, steady constant altitude flight at ~450 m altitude. These two fields appear to be anticorrelated at first glance. However, in the raw dataset, the correlation coefficient between T_z' and q_v' is -0.1648, which is significantly weaker than expected given the strong anticorrelations found in NS14. A possible reason for this is proposed here. In the DOMEX field campaign, aircraft data was collected at 1 Hz resolution while the aircraft flew at 90 m/s through the layer, corresponding to 1 measurement every 90 m. Because of this, it is assumed that each measurement is from a different air parcel, and each measurement is independent. The current study collects 1 Hz data as the air flows past the kite-borne sensors at 5-10 m/s, corresponding to one data point every 5-10 m apart. These measurements are hypothesized to be too close together to be unrelated, and the same assumption made for the DOMEX aircraft data cannot be made here. Therefore, high-frequency variations in temperature and humidity are likely to be positively correlated due to their close proximity. When the high-frequency variations are smoothed using a moving average filter with a span of 100 data points, then a correlation coefficient of -0.7679 is found between T_z' and q_v' during Flight 8 (Figure 20). This is consistent with the correlation coefficients found between T_z' and q_v' during the upstream flight leg in DOMEX, where the average was -0.78 across all research flights. T_z' and q_v' are also anticorrelated in the constant altitude portions of Flights 1, 2, and 4. In the raw datasets of each, the correlation coefficients lie between -0.45 and -0.65. These perturbations become more strongly anticorrelated (-0.9716, -0.8402, and -0.7174, respectively) when the high frequency

variations are smoothed, supporting the theory that the close proximity kite measurements are likely to be more positively correlated.

The vertical extent of the anticorrelated T_z' and q_v' patches is also investigated in the data collected from Flight 8, where reliable measurements were taken by multiple instruments simultaneously at different lengths along the kite string (Table 4). The strength of the anticorrelation appears to reach a maximum around roughly 417 m, but below this the correlation coefficient weakens. There is still some anticorrelation at roughly 374 m, but below 300 m there is almost no correlation at all between T_z' and q_v'. This is likely due to frictional interaction with the island underneath disturbing the incoming flow. This one example suggests that the anticorrelated variations are found in a relatively shallow layer, possibly 80-100 m deep. However, additional sampling is needed to attain a better estimate of the vertical extent. While a lower bound in the vertical extent of the anticorrelations is clear from the collected data, additional sensors attached to the kite string at smaller intervals will help improve an estimate of the lower bound. In addition, a longer kite line is needed in order to find an upper bound in the vertical extent of the anticorrelated patches, as the strength of the correlation does not decrease dramatically going upward from the ~417 m maximum in the collected data.

Strong negative correlation coefficients between T_z' and q_v' are found in only half of the kite observations containing a constant altitude portion. Flights 5, 6, 7, and 9 have weak, positive correlations between T_z' and q_v'. Possible reasons for this are discussed here. Flights 7 and 9 likely showed a weak correlation between T_z' and q_v' due to the location we flew at on these days. These two flights took place at Sandy Beach field, where the NE trade winds crossed over the island a significant distance before being measured (Figure 12). Therefore, it is highly likely that the incoming flow was already frictionally modified by the island terrain before being

measured by our kite-borne sensors. Because of this, the measurements on these days are not characteristic of the mixed marine boundary layer environment upstream of O‘ahu, so it is not surprising that convection “seeds” would not have been observed on these days. If the winds were easterly or southeasterly, or if we had deployed the instruments at a much higher altitude, we may have been able to capture the anticorrelations that were found on other flight days.

Although Flights 5 and 6 took place at Kaupō Beach, anticorrelations in T_z’ and q_v’ were not found on these days, likely due to the local and large scale weather conditions. Flight 5 took place on a cloudy day where the sky was 95% overcast at the observing location. Low clouds were present throughout the sampling period, and scattered precipitation fell just before the kite was launched. Flight 6 also took place on an overcast day with low clouds drifting overhead (Figure 25). During Flights 5 and 6, the kite-borne sensors took measurements just below cloud base as the kite itself flew through cloudy air multiple times. During Flight 6, the highest attached sensor entered a passing cloud at 450 m altitude. In both cases, it is likely that the kite measurements were influenced by the passage of low clouds and the presence of liquid water, which may have disturbed the air parcels as they were being measured. Air parcels in the presence of rain shafts require sufficient time to undergo buoyancy sorting as they drift through the mean flow. This was found in the aircraft datasets in NS14. The temperature and specific humidity perturbations from the aircraft measurements were not strongly anticorrelated during flights where liquid water was present, because buoyancy adjustment had not yet occurred. Once this buoyancy sorting has taken place, it is theorized that the T_z and q_v perturbations will be more strongly anticorrelated, as we are left with quasi-uniform density parcels that are cool/moist, and warm/dry. In flights 5 and 6, it is likely that the measured parcels had not yet adjusted after interaction with the cloudy air.

The large scale environment may have also played a role. 4 km resolution Infrared (IR) satellite imagery from the National Oceanic and Atmospheric Administration's (NOAA) Geostationary Operational Environmental Satellite (GOES) system, overlaid with output from the National Centers for Environmental Prediction (NCEP)'s Global Forecast System (GFS) model is provided below in order to show the large-scale weather conditions either shortly before or during several of our kite flights. GFS provides model output 4 times a day (00, 06, 12, and 18 UTC), so the images selected are those closest to our kite observation times. Figures 26-28 show satellite cloud top temperatures (°C) overlaid with surface winds and sea level pressure. Figures 26 and 27 show the large scale conditions on days where anticorrelated T_z' and q_v' patches are found (Flights 1, 2, 4, and 8). For comparison, Figure 28 shows the large-scale conditions on days where these anticorrelated patches are not found (Flights 5 and 6).

Figure 25. A photograph depicting the weather conditions at Kaupō Beach during Flight 6. Low clouds obscure a portion of the mountain downstream of the ambient trade wind flow.

a.)

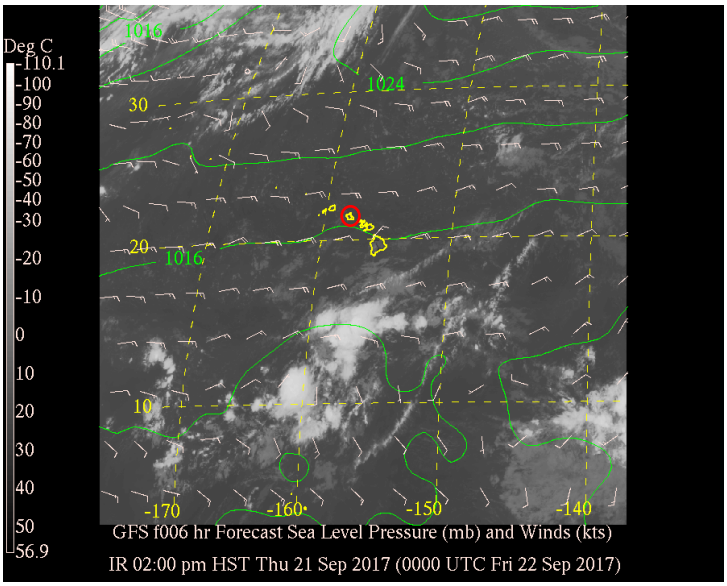

b.)

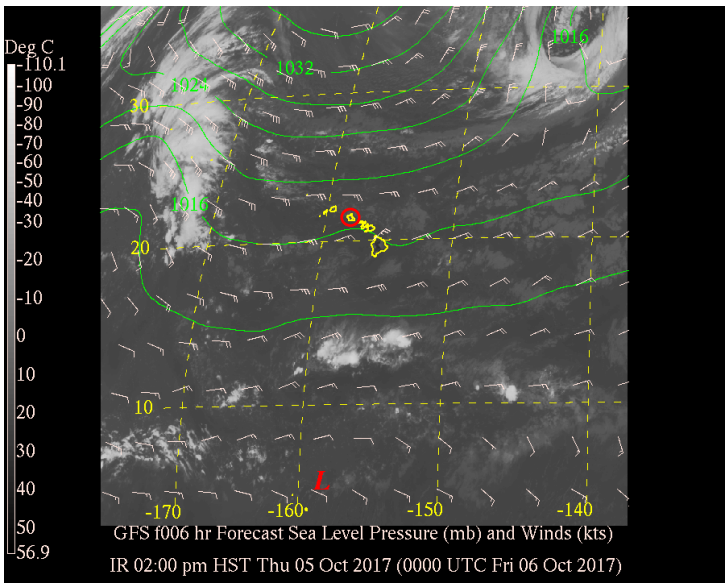

Figure 26. GOES-West 4 km IR Imagery with GFS model output overlaid, displaying satellite cloud top temperatures (°C), contoured sea level pressure (green, mb) and surface wind speed (wind barbs, kts). The latitude-longitude grid is marked by dashed yellow lines. The Hawaiian Islands are outlined in solid yellow, with O‘ahu circled in solid red. The positions of low and high pressure systems are labeled. a.) Ambient weather conditions are shown just prior to Flight 1 (2:00 PM HST, 9/21/2017) and b.) Flight 2 (2:00 PM HST, 10/5/2017).

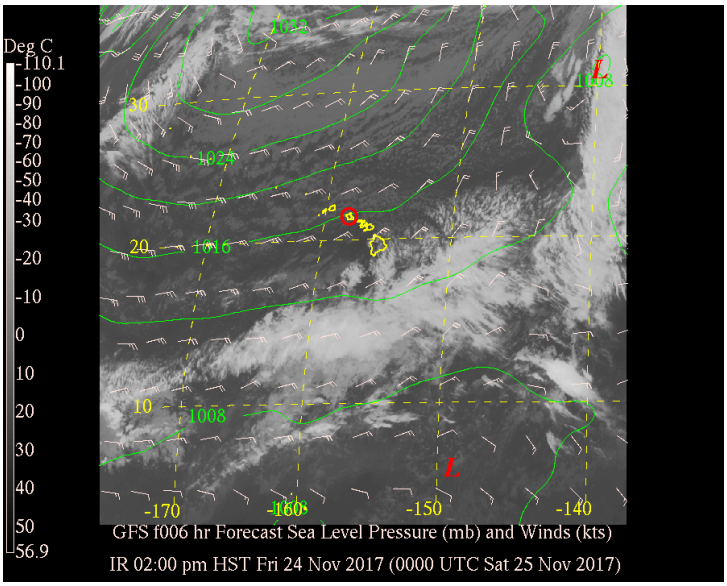

a.)

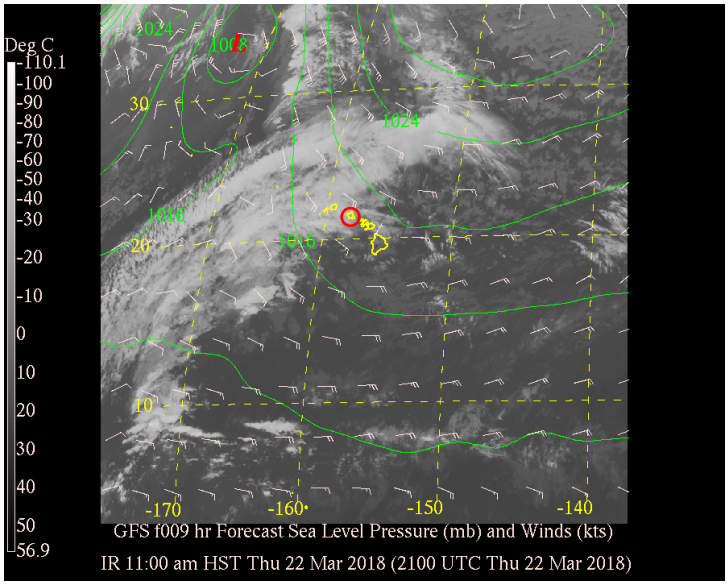

b.)

Figure 27. Same as in Figure 26. Ambient weather conditions are shown during Flight 4 (2:00 PM HST, 11/24/2017) and Flight 8 (11:00 AM HST, 3/22/2018).

a.)

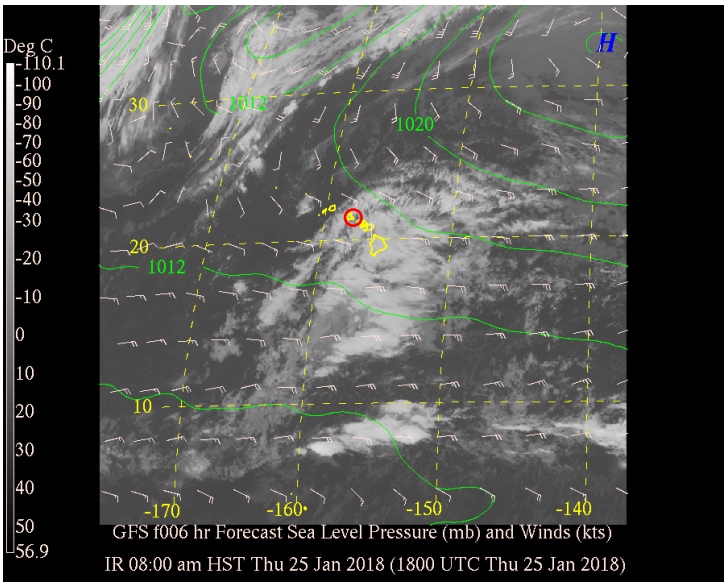

b.)

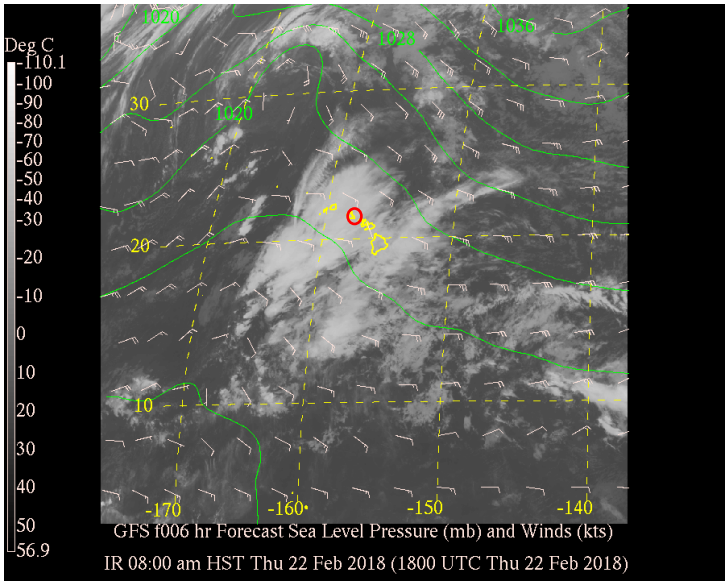

Figure 28. Same as in Figure 26. Ambient weather conditions are shown just prior to Flight 5 (8:00 AM HST, 1/25/2018) and Flight 6 (8:00 AM HST, 2/22/2018).

In Figures 28a and 28b, IR imagery reveals clouds both in the vicinity of and upstream of the Hawaiian Islands. This is not seen in Figures 26a, 26b, and 27a, where the upstream environment

is clear. Although Figure 27b (Flight 8) shows some clouds over Oʻahu, only mid-high level clouds were seen at Kaupō Beach during kite observation, and the upstream environment is relatively clear. In addition, the on-shore trade winds have a more easterly-northeasterly component during Flights 1, 2, 4, and 8, while they have a more southerly component during flights 5 and 6. In addition to the presence of clouds during flights 5 and 6, it is possible that the southeasterly winds may be causing the low level trade winds to become mixed as they pass the upstream Hawaiian Islands (Hawaiʻi, Maui, Molokaʻi, Lānaʻi, and Kahoʻolawe). This mixing may prevent parcels from having enough time to buoyancy sort before they are measured on Oʻahu. However, during Flight 8, the onshore winds came in from the east-southeast, placing the islands of Molokaʻi and Maui upstream of the sampling location. Despite this, anticorrelations were still found. Although this is a limited selection of flight days, it appears that the upstream environment may play a role in whether anticorrelated T_z' and q_v' patches can be observed. Low-level clouds that are present in the vicinity of or just upstream of the observing location may disturb parcels embedded in the flow. This may weaken the correlation between T_z' and q_v' as there may not be enough time for the parcels to undergo buoyancy adjustment.

It appears that several conditions must be met in order to observe moist "seeds" of convection. It was first hypothesized that long duration (~1 hour) sampling periods are needed, but strongly anticorrelated T_z and q_v perturbations were observed in a constant altitude flight as short as 11 minutes. However, longer duration constant altitude flights are preferred, as larger sample sets provide stronger evidence with better statistics. Additionally, in order to take measurements of the upstream flow, the wind direction needs to be coming entirely from offshore, unmodified by the land surface underneath or possibly the islands upstream. Steady, low-turbulence flow is necessary for reducing mixing and disturbance of the upstream

perturbations, as well as providing a suitable environment for flying kites. In addition, the presence of high moisture, cloudy air may be unfavorable for observing moist convection "seeds". The collected datasets must also be smoothed to remove positively correlated high frequency variations. For the datasets in which anticorrelated perturbations are observed, greater smoothing leads to stronger anticorrelations. The weather conditions favorable for using kites to measure the upstream marine boundary layer flow and studying convective initiation are more common during the Northern Hemisphere summer. During the summer, trade winds over the Hawaiian Islands are more consistent, steady, and easterly. However, kite sampling took place between September 2017 and April 2018, primarily during winter months due to the availability of instrumentation for the project. Three flights where anticorrelated perturbations were observed took place before winter, while the other successful flight took place in spring. The trade wind regime is less consistent in Hawai‘i during the winter due to large-scale interactions between tropical and migrating extra-tropical systems, as well as a stronger meridional temperature gradient.

4.2 Future Work

In this study we have laid the groundwork for future testing using kites by developing the necessary components and methods for making kite-based observations. In order to make firm conclusions about the use of kites in studying convective initiation, additional sampling and a larger sample set is needed. Our results so far are limited to a small set of testing days, and half of those days were unfavorable for studying convective initiation in the ambient upstream flow, in terms of either location or weather conditions. A larger sample set of kite flights is needed in order to make the current results easier to interpret. Further flights, especially during summer months, will allow for stronger conclusions to be made about the character and scale of moist

convection “seeds”. In addition, current and future kite datasets need to be combined with other observations and forecasts so that a broader array of questions can be applied. For example, how can we use kite-based observations to enhance understanding of processes that take place at sub-grid scales? Are we able to connect our observations of T_z’ and q_v’ to concurrent observations of cloud height, cloud width, or precipitation amount using the current convective initiation theory? These questions can be addressed with additional flights and longer sampling times. Further investigation into changes in convection and precipitation as a result of moist “seeds” being lifted over the island terrain is needed in order to verify their role in this process. This may be done by comparing the timing of moist “seed” observations with the timing of downstream convection and surface precipitation observations assuming advection timescales. In addition, the kite platform developed during this study will be used in future observations of the size distribution of sea salt aerosols.

REFERENCES

Anderson, P. S., 2003: Fine-scale structure observed in a stable atmospheric boundary layer by sodar and kite-borne tethersonde. *Boundary-Layer Meteorology, 107,* 323–351. https://doi.org/10.1023/A:1022171009297

Archibald, E. D., 1884: An account of some preliminary experiments with Biram's anemometers attached to kite strings or wires. *Nature, 31,* 66–8. https://doi.org/10.1038/031066a0

Balsley, B. B., Williams, J. B., Tyrrell, G. W., & Balsley, C. L., 1992: Atmospheric research using kites: Here we go again! *Bulletin of the American Meteorological Society, 73,* 17–30. https://doi.org/10.1175/1520-0477(1992)073%3C0017:ARUKHW%3E2.0.CO;2

Balsley, B. B., Jensen, M. L., & Frehlich, R. G., 1998: The use of state-of-the-art kites for the profiling the lower atmosphere. *Boundary-Layer Meteorology, 87,* 1–25. Retrieved from ftp://ftp.rap.ucar.edu/pub/rgf/kite_profiling.pdf

Balsley, B. B., Frehlich, R. G., Jensen, M. L., Meillier, Y., & Muschinski, A., 2003: Extreme gradients in the nighttime boundary layer: Structure, evolution, and potential causes. *Journal of the Atmospheric Sciences, 60,* 2496–2508. https://doi.org/10.1175/1520-0469(2003)060%3C2496:EGITNB%3E2.0.CO;2

Bain, C. L., Parker, D. J., Taylor, C. M., Kergoat, L., & Guichard, F., 2010: Observations of the nocturnal boundary layer associated with the West African monsoon. *Monthly Weather Review, 138,* 3142–3156. https://doi.org/10.1175/2010MWR3287.1

Daniels, P. A., and Oshiro, N. E., 1982: *Kahuku kite wind study. I. Kahuku beach boundary layer.* Manoa, HI: Department of Meteorology, University of Hawaii.

Espy, J. P., 1841: *The Philosophy of Storms.* Boston, MA: C.C. Little and J. Brown.

Fergusson, S. P., Alter, D., Dyke, R. A., & Blair, T. A., 1933: The early history of aerology in the United States. *Bulletin of the American Meteorological Society, 14(11),* 252–258. Retrieved from https://www.jstor.org/stable/26263240

Frankenfield, H. C., 1900: The Kite Work of the Weather Bureau. *Nature, 63,* 109–111. https://doi.org/10.1038/063109a0

Giambelluca, T. W., and Nullet, D., 1991: Influence of the trade-wind inversion on the climate of a leeward mountain slope in Hawaii. *Climate Research, 1,* 207–216. https://www.int-res.com/articles/cr/1/c001p207.pdf

Gold, E. and Harwood, W. A., 1909: The present state of our knowledge of the upper atmosphere as obtained by the use of kites, balloons, and pilot balloons. *Report of the British Association for the Advancement of Science,* 71–124.

Google. (n.d.). [Google Maps search for Oahu, Hawaii]. Retrieved June 27, 2018, from https://www.google.com/maps/@21.4840154,-158.1053125,11z

Hawaii State Energy Office. (n.d.). [Hawaii Renewable Energy Projects Directory: Kahuku Wind Farm]. Retrieved June 26, 2018, from https://energy.ehawaii.gov/epd/public/energy-project-details.html?rid=27--33890ffdee6938f

Knapp, K. G., Jensen, M. L., Balsley, B. B., Bognar, J. A., Oltmans, S. J., Smith, T. W., & Birks, J. W., 1998: Vertical profiling using a complementary kite and tethered balloon platform at Ferryland Downs, Newfoundland, Canada: Observation of a dry, ozone-rich plume in the free troposphere. *Journal of Geophysical Research: Atmospheres, 103,* 13389–13397. https://doi.org/10.1029/97JD01831

Lau, K. M., and Wu, H. T., 2003: Warm rain processes over tropical oceans and climate implications. *Geophysical Research Letters, 30(24),* 2290. https://doi.org/10.1029/2003GL018567

McAdie, A., 1892: Experiments on atmospheric electricity made by direction of the chief of the Weather Bureau at Blue Hill Meteorological Observatory, July 12–August 12, 1892. *Annals of the Astronomical Observatory of Harvard College, 40,* 120–124.

McAdie, A., 1917: *The principles of aerography.* Boston, MA: Rand McNally & Company. https://doi.org/10.1038/105479a0

National Centers for Environmental Information (n.d.). [Geostationary Operational Environmental Satellite 4 km IR Imagery: State of Hawaii. Model output overlay from the National Centers for Environmental Prediction Global Forecast System]. Retrieved June 28, 2018, from http://mkwc.ifa.hawaii.edu/archive/satellite/index.cgi

Nugent, A. D., & Smith, R. B., 2014: Initiating moist convection in an inhomogeneous layer by uniform ascent. *Journal of the Atmospheric Sciences, 71(12),* 4597–4610. https://doi.org/10.1175/JAS-D-14-0089.1

Reiche, M., Funk, R., Zhang, Z., Hoffmann, C., Li, Y., & Sommer, M., 2012: Using a parafoil kite for measurement of variations in particulate matter—a kite-based dust profiling approach. *Atmospheric and Climate Sciences, 2(1),* 41–51. http://dx.doi.org/10.4236/acs.2012.21006

Varney, G. J., 1898, May: Kite-flying in 1897. *Popular Science Monthly, 53,* 48–63.

Wiche, S. A., 1992: Weather on a string. *Weatherwise, 45(3),* 10–16. https://doi.org/10.1080/00431672.1992.9930190

Winning, Jr. T. E., Chen, Y.-L., & Xie, F., 2016: Estimation of the marine boundary layer height over the central North Pacific using GPS radio occultation. *Atmospheric Research, 183(1),* 362–370. https://doi.org/10.1016/j.atmosres.2016.08.005

Woodcock, A. H., 1960: The origin of trade-wind orographic shower rains. *Tellus A: Dynamic Meteorology and Oceanography, 12(3),* 315–326. doi:10.1111/ j.2153-3490.1960.tb01316.x